

1

2

3 Non-proliferative adult neurogenesis in neural crest-derived stem
4 cells isolated from human periodontal ligament.

5

6

7

8 **Authors:** Carlos Bueno^{1*}, Marta Martínez-Morga² and Salvador Martínez¹.

9

10 ¹ Instituto de Neurociencias de Alicante (UMH-CSIC), San Juan, Alicante, 03550,
11 Spain.

12 ² Department of Human Anatomy and Institute of Biomedical Research (IMIB),
13 University of Murcia, Faculty of Medicine, Murcia, 30800, Spain.

14

15

16 *Corresponding author: Carlos Bueno, PhD., E-mail: cbueno@umh.es

17 Marta Martínez-Morga: m.martinezmorga@um.es

18 Salvador Martínez: smartinez@umh.es

19

20 **Abstract**

21 **Background:** Self-renewal and lineage regulation of neural stem cells in the adult
22 mammalian brain (aNSCs) are still far from been understood. Although previous studies
23 have reported that some aNSCs in neurogenic niches showed irregular nuclei, their
24 functional significance remains elusive. We used neural crest-derived human periodontal
25 ligament stem cells (hPDLSCs) as an in vitro cell model of neurogenesis to investigate
26 the functional significance of nuclear polymorphisms.

27 **Results:** Here, we show that hPDLSCs-derived neurons are not directly generated
28 through cell division from stem cells. In fact, the cell shape of neural precursors is reset
29 and start their neuronal development as round spheres. The hPDLSCs-derived neurons
30 gradually adopted a complex morphology by forming several processes, that grew and
31 arborized, acquiring dendritic-like and axonal-like identities, giving rise to a variety of
32 neuron-like morphologies. To our knowledge, this article provides the first observation
33 of these morphological events during in vitro neurogenesis and neuron polarization in
34 human aNCSCs, and we have discovered a transient cell nuclei lobulation coincident to
35 in vitro neurogenesis, without being related to cell proliferation. We observed that small
36 DNA containing structures move within the cell to specific directions and temporarily
37 form lobed nuclei. Morphological analysis also reveals that neurogenic niches in the adult
38 mouse brain contains cells with nuclear shapes highly similar to those observed during in
39 vitro neurogenesis from hPDLSCs.

40 **Conclusions:** Our results provide strong evidence that neuronal differentiation from
41 aNSCs may also occur during in vivo adult mammalian neurogenesis without being
42 related to cell proliferation. In addition, we demonstrate that hPDLSCs-derived neurons
43 display a sequence of morphologic development highly similar to those observed in
44 primary neuronal cultures derived from rodent brains during neurogenesis, providing

45 strong evidence that it is possible to reproduce neurogenic processes and obtain neurons
46 from hPDLSCs. Beyond the central nervous system, the presence of lobed nuclei has been
47 reported in most blood and immune cells, but the functional significance of multilobed
48 nuclear structures is not yet established. Our results suggest that multilobed nuclear
49 structures is associated to nuclear movement within the cell.

50

51 **Keywords:** Neurogenesis; neuronal polarity; neural stem cells; neural crest stem cells;
52 adult stem cells; human periodontal ligament stem cells; nucleus; nuclear remodeling;
53 micronuclei.

54

55 **Background**

56 Neural stem cells (NSCs) are multipotent populations of undifferentiated cells present
57 both during development and in the adult central nervous system that give rise to new
58 neurons and glia [1]. The presence of neural stem cells in the adult mammalian brain
59 (aNSCs) have been described in two neurogenic niches, the ventricular-subventricular
60 zone (V-SVZ) of the anterolateral ventricle wall and the subgranular zone (SGZ) of the
61 hippocampal dentate gyrus [2-9].

62 The study of the cell composition of neurogenic niches and the use of methods for
63 detecting proliferating cells, suggest that neurogenesis occurs progressively through
64 sequential phases of proliferation and the neuronal differentiation of aNSCs.

65 In the V-SVZ, putative aNSCs (type B cells) divide to give rise to intermediate progenitor
66 cells (type C cells), which divide a few times before becoming neuroblasts (type A cells).
67 The neuroblast then migrate into the olfactory bulb and differentiate into distinct types of
68 neurons [2-4]. In the SGZ, putative aNSCs (type 1 cells) divide to give rise to intermediate

69 progenitor cells (type-2 cells) which exhibit limited rounds of proliferation before
70 generating polarized neuroblast (type-3 cells) [5-9]. Neuroblast, as polarized cells, then
71 migrate, guided by the leading process, along SGZ and differentiate into dentate granule
72 neurons [10, 11].

73 However, only one of the studies suggesting that neurogenesis occurs progressively
74 through sequential phases of proliferation [2-9] showed mitotic chromosomes [8]. In
75 addition, the self-renewal and multipotent properties demonstrated by NSC *in vitro* [12]
76 have not been clearly demonstrated *in vivo* [10,13,14].

77 Ultrastructure and immunocytochemistry studies show that the V-SVZ stem cell niche
78 contains cells with irregular (polymorphic) nuclei [15-17]. Type-B cells have irregular
79 nuclei that frequently contain invaginations. Type-C cells nuclei contain deep
80 invaginations and Type-A cell nuclei are also occasionally invaginated [2]. Furthermore,
81 recent studies have shown that murine and human V-SVZ contains cells with segmented
82 nuclei connected by an internuclear bridge [18-20]. Although it has been suggested that
83 these are associated with quiescence in aNSCs [20], the functional significance of
84 different nuclear morphologies remains elusive.

85 Ultrastructure and immunocytochemistry studies also show that the SGZ stem cell niche
86 contains cells with irregular (polymorphic) nuclei [21-28]. Type-2 cells had an irregularly
87 shaped nucleus [7,9]. In addition, one study found that many cultured hippocampal
88 neurons have irregular nuclei or even consisted of two or more lobes connected by an
89 internuclear bridge [29].

90 Moreover, how neuroblasts acquire the appropriate cell polarity to initiate their migration
91 remains unclear [30]. The process of neuronal polarization has been studied for decades
92 using dissociated rodent embryonic hippocampal pyramidal neurons and postnatal

93 cerebellar granule neurons in culture [31,32]. During neuronal polarization *in vitro*, the
94 morphological changes in cultured neurons are divided into different stages.

95 Upon isolation, dissociated pyramidal neurons retract their processes, so that their
96 development *in vitro* begins as rounded spheres that spread lamellipodia (stage 1). These
97 spheres appear symmetrical, extending and retracting several immature neurites of a
98 similar length (stage 2). Elongation of a single process, that which presumably becomes
99 the axon, breaks this symmetry (stage 3). The next step involves the remaining short
100 neurites morphologically developing into dendrites (stage 4) and the functional
101 polarization of axon and dendrites (stage 5), including dendritic spine and synapse
102 formation [33]. Dissociated granule neurons also present a lamellipodia after attaching to
103 the substratum (stage 1). These spheres extend a unipolar process at a single site on the
104 plasma membrane (stage 2) followed by extension of a second process from the opposite
105 side of the cell body, resulting in a bipolar morphology (stage 3). One of the two axon
106 elongates further and start branching (stage 4), and shorter dendritic processes develop
107 around the cell body (stage 5) [34].

108 Understanding the sequence of events from aNSCs to neuron is not only important for the
109 basic knowledge of NSCs biology, but also for therapeutic applications [35]. The major
110 barrier to studying human aNSCs is the inaccessibility of living tissue, therefore an
111 enormous effort has been made in this study to derive neurons from human stem cells
112 [36]. *In vitro* models of adult neurogenesis mainly utilize fetal, postnatal and adult NSCs
113 [37]. Neural crest stem cells (NCSCs) are a migratory cell population that generate
114 numerous cell lineages during development, including neurons and glia [38,39]. NCSCs
115 are present not only in the embryonic neural crest, but also in various neural crest-derived
116 tissues in the fetal and even adult organs [40]. The periodontal ligament (PDL) is a
117 connective tissue surrounding the tooth root that contains a source of human NCSCs

118 which can be accessed with minimal technical requirements and little inconvenience to
119 the donor [41]. Isolation and characterization of multipotent stem cells from the human
120 PDL have been previously described [42, 43].

121 In previous publication, we showed that several stem cell and neural crest cell markers
122 are expressed in human adult periodontal ligament (hPDL) tissue and hPDL-derived cells.

123 *In vitro*, hPDL-derived cells differentiate into neural-like cells based on cellular
124 morphology and neural marker expression. *In vivo*, hPDL-derived cells survive, migrate
125 and expressed neural markers after being grafted to the adult mouse brain. Moreover,
126 some hPDL-derived cells graft into stem cell niches such as V-SVZ of the anterolateral
127 ventricle wall and the SGZ of the dentate gyrus in the hippocampus. The hPDL-derived
128 cells located in the stem cell niches show neural stem morphology [44]. Moreover,
129 hPDLSCs cells displayed inward currents conducted through voltage-gated sodium (Na⁺)
130 channels and spontaneous electrical activities after neurogenic differentiation [45, 46].
131 Therefore, the neural crest origin and neural potential make human periodontal ligament
132 stem cells (hPDLSCs) interesting as an *in vitro* human cell model of neurogenesis for
133 investigating aNSCs to neuron differentiation mechanisms.

134 Here, we show that hPDLSCs-derived neurons are not directly generated through cell
135 division from stem cells. In fact, the cell shape of neural precursors is reset and start their
136 neuronal development as round spheres. To our knowledge, this article provides the first
137 observation of these morphological events during *in vitro* neurogenesis and neuron
138 polarization in human aNCSCs, and we have discovered a transient cell nuclei lobulation
139 coincident to *in vitro* neurogenesis, without being related to cell proliferation. We
140 observed that small DNA containing structures move within the cell to specific directions
141 and temporarily form lobed nuclei.

142 Morphological analysis also reveals that the V-SVZ of the anterolateral ventricle wall and
143 the SGZ of the hippocampal dentate gyrus in the adult mouse brain contains cells with
144 nuclear shapes highly similar to those observed during *in vitro* neurogenesis from
145 hPDLSCs, suggesting that neuronal differentiation from aNSCs may also occur during *in*
146 *vivo* adult mammalian neurogenesis without being related to cell proliferation.

147 In addition, morphological analysis revealed that hPDLSCs-derived neurons display a
148 sequence of morphologic development highly similar to those observed in primary
149 neuronal cultures derived from rodent brains during neurogenesis, providing strong
150 evidence that it is possible to reproduce neurogenic processes and obtain neurons from
151 hPDLSCs.

152 Although previous studies have reported the presence of lobed nuclei in most blood and
153 immune cells, their functional significance remains elusive. Our results suggest that
154 multilobed nuclear structures is associated to nuclear movement within the cell.

155

156 **Materials and methods**

157 **Cell Culture**

158 Human premolars were extracted and collected from healthy donors undergoing
159 orthodontic therapy in Murcia dental hospital (Spain). hPDL was scraped from the middle
160 third region of the root surface. After washing the extracted PDL with Ca and Mg-free
161 Hank's balance salt solution (HBSS; Gibco), hPDL was digested with 3 mg/ml type I
162 collagenase (Worthington Biochemical Corporation) and 4 mg/ml dispase II (Gibco) in
163 alpha modification minimum essential medium eagle (α -MEM) (α -MEM; Sigma-
164 Aldrich) for 1 h at 37°C. The reaction was stopped by the addition of α -MEM. The

165 dissociated tissue was passed through a 70- μ m cell strainer (BD Falcon). Cells were
166 centrifuged, and the pellet was resuspended in in serum-containing media (designated as
167 the basal media), composed of α -MEM supplemented with 15% calf serum (Sigma), 100
168 units/ml penicillin-streptomycin (Sigma) and 2 mM l-glutamine (Sigma). The cell
169 suspension was plated into six-well multiwell plates (BD Falcon) and incubated at 37°C
170 in 5% CO₂. To induce neural differentiation, cells were cultured in serum-free media
171 (designated as the neural induction media), consisting in Dulbecco's modified Eagle's
172 medium/F12 (DMEM/F12, Gibco) supplemented with bFGF (20 ng/ml, R&D Systems),
173 EGF (20 ng/ml, R&D Systems), glucose (0.8 mg/ml, Sigma), N2-supplement (Gibco), 2
174 mM l-glutamine (Sigma), and 100 units/ml penicillin-streptomycin (Sigma). Neural
175 induction media were changed every 3-4 days until the end of the experiment (2 weeks).

176 **Immunocytochemistry**

177 Cells were plated onto coated plastic or glass coverslips, and maintained in basal media
178 or neural induction media. Cells were rinsed with PBS and fixed in freshly prepared 4%
179 paraformaldehyde (PFA; Sigma). Fixed cells were blocked for 1 h in PBS containing 10%
180 normal horse serum (Gibco) and 0.25% Triton X-100 (Sigma) and incubated overnight at
181 4°C with antibodies against: β -III-tubulin (TUJ1; 1:500, Covance), Connexin-43 (3512;
182 1/300, Cell Signalling), Synaptophysin (18-0130; 1/300, Zymed), Synapsin1 (NB300-
183 104; 1/300, Novus), Fibrillarin (ab5821; 1/300, Abcam) and Laminin A/C (GTX101127;
184 1/300, GeneTex) in PBS containing 1% normal horse serum and 0.25% Triton X-100. On
185 the next day, cells were rinsed and incubated with the corresponding secondary
186 antibodies: Alexa Fluor® 488 (anti-mouse or anti-rabbit; 1:500, Molecular Probes),
187 Alexa Fluor® 594 (anti-mouse or anti-rabbit; 1:500, Molecular Probes), biotinylated anti-
188 rabbit (BA1000, 1:250; Vector Laboratories), biotinylated anti-chicken (BA9010, 1:250,
189 Vector Laboratories, CY3-streptavidin (1:500, GE Healthcare). Cell nuclei were

190 counterstained with DAPI (0.2 mg/ml in PBS, Molecular Probes). Alexa Fluor 488®
191 phalloidin was used to selectively stains F-actin (Molecular Probes).

192 **Western Blotting**

193 hPDL-derived cells were harvested using trypsin/EDTA (Gibco), washed twice with PBS,
194 resuspended in RIPA lysis buffer (Millipore) for 30 min at 4°C in the presence of protease
195 inhibitors (Pierce™. protease inhibitor Mini Tables, Pierce Biotechnology Inc) and PMSF
196 1M (Abcam). Protein concentration was determined using the Bradford protein assay
197 (Sigma-Aldrich). Proteins were separated in 8% SDS-polyacrylamide gel (PAGE-SDS)
198 and transferred to a nitrocellulose membrane (Whatman). PageRuler™ Prestained Protein
199 Ladder (Thermo Scientific) has been used as size standards in protein electrophoresis
200 (SDS-PAGE) and western-blotting. After transfer, nitrocellulose membranes were
201 stained with Ponceau S solution (Sigma-Aldrich) to visualize protein bands. Blots were
202 then incubated over-night at 4°C with rabbit antibody against β -III-tubulin (TUJ1;
203 1:1000, Covance). Secondary antibody was used at 1:7000 for peroxidase anti-mouse Ab
204 (PI-2000, Vector Laboratories). Immunoreactivity was detected using the enhanced
205 chemiluminescence (ECL) Western blot detection system (Amersham Biosciences
206 Europe) and Luminata™ Forte (Millipore corporation) using ImageQuant LAS 500 Gel
207 Documentation System (GE Healthcare). The molecular weight of β -III-tubulin is
208 approximately 55 kDa.

209 **Immunohistochemistry**

210 Experiments were carried out according to the guidelines of the European Community
211 (Directive 86/609/ECC) and in accordance with the Society for Neuroscience
212 recommendations. Animals used in this study were 12-week-old immune-suppressed
213 mouse (Hsd: Athymic Nude-Foxn1 nu/nu; Harlan Laboratories Models, S.L), housed in a

214 temperature and humidity controlled room, under a 12h light/dark cycles, with *ad libitum*
215 access to food and water. The animals were anesthetized and intracardially perfused with
216 freshly prepared, buffered 4% PFA (in 0.1M PB, pH 7.4). Brains were removed, post-
217 fixed for 12 hr in the same fixative at 4°C and dehydrated in 30% sucrose solution at 4°C
218 until sunk. 30µm thick coronal sections were collected using a freezing microtome. Serial
219 sections were used for DAPI staining. Free-floating sections were incubated and mounted
220 onto Superfrost Plus glass slides (Thermo Scientific). The slides were dried O/N and
221 coverslipped with mowiol-NPG (Calbiochem).

222 **Images and Data Analyses**

223 Analyses and photography of visible and fluorescent stained samples were carried out in
224 an inverted Leica DM IRB microscope equipped with a digital camera Leica DFC350FX
225 (Nussloch) or in confocal laser scanning microscope Leica TCS-SP8. Digitized images
226 were analyzed using LASX Leica confocal software. Z-stacks of confocal fluorescent
227 images were also analyzed to calculate the nuclear volume by using ImageJ software.

228 **Scanning Electron Microscopy**

229 Cells were plated onto coated glass coverslips and maintained in basal media or neural
230 induction media. Cells were treated with fixative for 20 minutes. Coverslips were
231 postfixed in 1% osmium tetroxide for 1 hour and dehydrated in graded ethanol washes.
232 The coverslips were allowed to dry at a conventional critical point and were then coated
233 with gold-palladium sputter coated. Coverslips were view on a Jeol 6100 scanning
234 electron microscope.

235

236

237 **Results**

238 As noted in the introduction, the aim of this work was to evaluate the sequence of
239 biological events occurring during the neural differentiation of hPDLSCs. Morphological
240 characteristics of the hPDLSCs, including cell shape, cell surface features, cytoskeleton,
241 and nuclear morphology were examined in cells under proliferation and neural
242 differentiation conditions.

243 **hPDLSCs cultured in basal media**

244 Under proliferation conditions, hPDLSCs displayed a fibroblast-like morphology with
245 low-density microvilli on the cell surface (Fig. 1a) and actin microfilaments and β -III
246 tubulin microtubules oriented parallel to the longitudinal axis of the cell (Fig. 1b). The
247 cytoskeletal protein class III beta-tubulin isotype is widely regarded as a neuronal marker
248 in developmental neurobiology and stem cell research [47]. Dental and oral-derived stem
249 cells displayed spontaneous expression of neural marker β -III tubulin, even without
250 having been subjected to neural induction [48]. Western blot analysis verified the
251 expression of β -III tubulin in hPDLSCs (Fig. 1c). During mitosis, β -III tubulin is present
252 in the mitotic spindle and it is detectable in all phases of mitosis (Fig. 1d). The cytoskeletal
253 protein class III beta-tubulin isotype is a component of the mitotic spindle in multiple cell
254 types [49]. During interphase, undifferentiated hPDLSCs displayed a flattened,
255 ellipsoidal nucleus, often located in the center of the cell and with a nuclear volume
256 around $925'356 \pm 52'6184 \mu\text{m}^3$ (Fig. 1e).

257 **hPDLSCs cultured in neural induction media**

258 After 14 days of neural differentiation conditions, the hPDLSCs displayed different
259 morphologies, including round cells with small phase-bright cell bodies and short

260 processes; highly irregularly-shaped cells; and, also, unipolar, bipolar and multipolar-
261 shaped cells with small phase-bright cell bodies and multiple branched processes (Fig.
262 1f). In addition, cells of different size were also observed (Fig. 1g). Furthermore,
263 microscopic analysis revealed that some hPDLSCs have different nuclear shapes,
264 including lobed nuclei connected by an internuclear bridge (Fig. 1h). The results indicate
265 that the cell culture simultaneously contains hPDLSCs at different stages of neurogenesis
266 and neuronal polatization. We acknowledge that the definitive sequence of *in vitro*
267 neurogenesis and neuronal polarization from hPDLSCs will be provided only by time-
268 lapse microscopy of a single cell, but in our experimental conditions, several pieces of
269 data suggest how these steps may occur.

270 ***In vitro* neurogenesis from hPDLSCs**

271 After neural induction, hPDLSCs undergo a dramatic change in shape and size, first
272 adopting highly irregular forms and then gradually contracting into round cells with small
273 phase-bright cell bodies (Fig. 2a). Cytoskeletal remodeling is observed during the
274 morphological changes that occurred when the hPDLSCs round up to a near-spherical
275 shape. Actin microfilament not longer surround the nucleus and became cortical. Unlike
276 actin, β -III tubulin seems to accumulate around the nucleus (Fig. 2b). Actin microfilament
277 and β -III tubulin microtubule network are almost lost in the rounded cells (Fig. 2c).
278 Scanning electron micrographs show that hPDLSCs also experience dramatic changes in
279 cell surface features. Under proliferation conditions, hPDLSCs remain very flat,
280 presenting low-density microvilli on their surface (Fig. 1a), but there is a marked increase
281 in the number of microvilli as the cells round up to near-spherical shape (Fig. 2d). The
282 surface of the round cells is almost devoid of microvilli (Fig. 2e). Cytokinesis and mitotic
283 spindle were not observed during the described of *in vitro* neurogenesis processes (Fig.
284 1f-h, 2).

285 **Neuronal polarization of hPDLSCs-derived neurons**

286 Morphological analysis revealed that hPDLSCs-derived neurons display a sequence of
287 morphologic development highly similar to those observed in dissociated-cell cultures
288 prepared from rodent brain (Fig. 3-5). hPDLSCs-derived neurons also start their
289 development as rounded spheres that initiated neurite outgrowth at a single site on the
290 plasma membrane, first becoming unipolar, stages 1-2 (Fig. 3a). We did not observe the
291 development of lamellipodia around the circumference of the cell body. These unipolar
292 cells, later transformed into cells containing several short neurites, developed around the
293 cell body, stage 3 (Fig. 3b). An analysis of the cytoskeletal organization during spherical
294 stages of hPDLSCs-derived neurons showed that the β -III tubulin microtubules and actin
295 microfilament network is reorganized. Cytoskeletal protein β -III tubulin was densely
296 accumulated under the cell membrane of the hPDLSCs-derived neurons cell bodies and
297 in cell neurites (Fig. 3a,b) while actin microfilaments were mainly found in cell neurites
298 (Fig. 3c). We observed that hPDLSCs-derived neurons produce neurites that showed
299 growth cone formations at their tips (Fig. 3c-e). The central domain of the growth cone
300 contains β -III tubulin microtubules and the peripheral domain is composed of radial F-
301 actin bundles (Fig. 3d), similar to the typical spatial organization described in neurons
302 [50, 51]. Scanning electron micrographs also showed that the growth cone of hPDLSCs-
303 derived neurons contained filopodia and vesicles on the cell surface (Fig. 3e). These
304 findings are consistent with a previous study reporting that membrane addition and
305 extension in growth cones is mediated by diverse mechanism, including exocytosis of
306 vesicular components [52].

307 At later stages of differentiation, the hPDLSCs-derived neurons gradually adopted a
308 complex morphology by forming several processes, stage 4 (Fig. 3f) that grew and
309 arborized, acquiring dendritic-like and axonal-like identities, giving rise to a variety of

310 neuron-like morphologies (Fig. 3g). The next step, stage 5, in neuronal polarization from
311 rodent neurons in culture is the functional polarization of axon and dendrites, including
312 dendritic spine formation and axon branch formation. Dendritic spines are micron-sized
313 dendrite membrane protrusions [53]. Depending on the relative sizes of the spine head
314 and neck, they can be subdivided into different categories, including filopodium,
315 mushroom, thin, stubby, and branched spines [54]. Dendritic spines are actin-rich
316 compartments that protrude from the microtubule-rich dendritic shafts of principal
317 neurons [55]. Based on morphology, complexity, and function, axon branching is grouped
318 into different categories, including arborization, bifurcation, and collateral formation
319 [56].

320 Our morphological analysis revealed that hPDLSCs-derived neurons developed well-
321 differentiated axonal-like and dendritic-like domains. These types of processes differ
322 from each other in morphology (Fig. 3h-4d). Cytoskeletal protein β -III tubulin and F-
323 actin staining showed that the hPDLSCs-derived neurons comprised multiple branched
324 dendrite-like processes with dendritic spines-like structures (Fig. 3h). Scanning electron
325 micrographs showed that the hPDLSCs-derived neurons also contained multiple
326 branched dendrite-like processes with variously shaped spine-like protrusions, highly
327 similar to filopodium, mushroom, thin, stubby, and branched dendritic spines shapes (Fig.
328 4a). Furthermore, hPDLSCs-derived neurons also displayed different types of axonal
329 branch-like structures, including bifurcation (Fig. 4b), arborization (Fig. 4c), and
330 collateral formation (Fig. 4d).

331 The last step in neuronal polarization from rodent neurons in culture is synapse formation.
332 The most frequent types of synaptic communication include axodendritic, axosomatic,
333 axoaxonic and dendrodendritic synapses. Morphological analysis revealed that the
334 hPDLSCs-derived neurons connected to one another (Fig. 5a) through different types of

335 synapse-like interactions, including dendrodendritic-like, axoaxonic-like and
336 axodendritic-like synapses (Fig. 5b). Synapse-associated proteins Cx43, Synaptophysin
337 and Synapsin1 were found accumulated in the cell surface of neurites (Fig. 5c).

338 **Nuclear remodeling**

339 Nuclear morphology was examined in hPDLSCs under proliferation and neural
340 differentiation conditions. The dynamic localization of the nucleoli was analyzed by
341 immunostaining for fibrillarin, the main component of the active transcription centers
342 [57] and the dynamic localization of the nuclear lamina was analyzed by immunostaining
343 for laminin A/C, a nuclear lamina component [58].

344 As noted above, during interphase, hPDLSCs displayed a flattened, ellipsoidal nucleus,
345 often located in the center of the cell, and with a nuclear volume around $925'356$
346 $\pm 52'6184\mu\text{m}^3$ (Fig. 1e). The nuclei of hPDLSCs contained two or more nucleoli and the
347 inside surface of the nuclear envelope is lined with the nuclear lamina (Fig. 6a).

348 Previous studies have shown that the nuclear lamina and nucleolus are reversibly
349 disassembled during mitosis [59, 60]. Microscopic analysis of hPDLSCs revealed that the
350 dynamic localization of fibrillarin and laminin A/C proteins during mitosis are similar to
351 those observed in previous studies (Fig. 6b).

352 Morphological analysis also revealed that nuclear remodeling occurred during *in vitro*
353 neurogenesis from hPDLSCs (Fig. 7-10). We acknowledge that the definitive sequence
354 of nuclear remodeling when hPDLSCs round up to near-spherical shape will only be
355 provided by time-lapse microscopy, but our accumulated data suggests how these steps
356 may occur.

357 Small DNA containing structures start to move towards specific positions within the cell
358 (Fig. 7a-n) and temporarily form lobed nuclei (Fig. 7o-r). Later, these lobed nuclei

359 connected to one another through small DNA containing structures (Fig. 7s-x) forming
360 internuclear bridges (Fig. 7y-8j). Finally, there is restoration of irregular, but non-lobed,
361 nucleus with an eccentric position within hPDLSCs-derived neurons (Fig. 8k-o). These
362 small DNA containing structures displayed a spherical or ovoid shape (Fig. 9a), and it
363 seems that some of them are connected to the main body of the nucleus by thin strands of
364 nuclear material (Fig. 9b). Fibrillarin and laminin A/C proteins were detected in these
365 small DNA containing structures (Fig. 10a). The nuclear lamina and nucleolus are not
366 disassembled during *in vitro* neurogenesis from hPDLSCs (Fig. 10b).

367 No lobed nuclei were observed as PDL-derived neurons gradually acquired a more mature
368 neuronal-like morphology (Fig. 11a). We also found that as the cells round up to a near-
369 spherical shape the nuclear volume of the hPDLSCs decreases to an approximate volume
370 of $279'589 \pm 38'8905 \mu\text{m}^3$ (Fig. 11b). Cytokinesis, mitotic chromosomes and mitotic
371 spindle were not observed during the described of *in vitro* neurogenesis processes or
372 neuronal polarization from hPDLSCs (Fig. 7-11).

373 Interestingly, the morphological analysis revealed that the adult rodent V-SVZ of the
374 anterolateral ventricle wall (Fig. 12a) and the SGZ of the hippocampal dentate gyrus (Fig.
375 12b), where adult neurogenesis has been clearly demonstrated, contained abundant cells
376 with nuclear shapes highly similar to those observed during *in vitro* neurogenesis from
377 hPDLSCs. Although it has been suggested that lobed nuclei connected by an internuclear
378 bridge are associated with quiescence in aNSCs [20], we observed that this kind of nuclei
379 is associated to nuclear movement within the cell during initial phases of neurogenesis,
380 without being related to cell proliferation.

381

382

383 Discussion

384 It has commonly been assumed that adult neurogenesis occurs progressively through
385 sequential phases of proliferation [10,11]. However, there are almost no studies that show
386 mitotic chromosomes or mitotic spindle to really confirm that this really happens [2-9].
387 In addition, the self-renewal and multipotent properties demonstrated by NSC *in vitro*
388 [12] have not been clearly demonstrated *in vivo* [10,13,14].

389 Despite the advantages for the detection of adult neurogenesis using exogenous
390 thymidine analog administration or endogenous cell cycle markers, in addition to cell
391 stage and lineage commitment markers, recent findings indicate that some observations
392 interpreted as cell division could be normal DNA turnover or DNA repair [61,62,63].
393 Thymidine analogs such as tritiated thymidine and BrdU may also be incorporated during
394 DNA synthesis that is not related to cell proliferation [64, 65]. Proliferating cell nuclear
395 antigen is also involved in DNA repair [66]. Positivity of the proliferation marker KI-67
396 in noncycling cells has also been observed [67].

397 Previous ultrastructure and immunocytochemistry studies also show that the V-SVZ stem
398 cell niche contains cells with different morphologies and irregular nuclei [2-4,15-20].
399 Type-B cells have irregular nuclei that frequently contain invaginations and irregular
400 contours of the plasma membrane. Type-C cells nuclei contained deep invaginations and
401 these cells are more spherical. Type-A cells have elongated cell body with one or two
402 processes and the nuclei are occasionally invaginated [2]. Furthermore, some studies have
403 shown that murine and human V-SVZ have segmented nuclei connected by an
404 internuclear bridge [18-20].

405 In addition, previous reports also shown irregular shaped nuclei in the adult SGZ [21-28].
406 Adult SGZ NSCs (type 1 cells) have irregular contours of the plasma membrane, and

407 differences in heterochromatin aggregation has been also observed [9]. Adult SGZ NSCs
408 (type 2 cells) had an irregularly shaped nucleus [11, 13]. Furthermore, one study found
409 that many cultured hippocampal neurons have irregular nuclei or even consisted of two
410 or more lobes connected by an internuclear bridge [29].

411 In this study, we show that hPDLSCs-derived neurons are not directly generated through
412 cell division from stem cells. The undifferentiated polygonal and fusiform cell shapes are
413 reset and start their neuronal development as rounded spheres. The hPDLSCs-derived
414 neurons gradually adopted a complex morphology by forming several processes, that
415 grew and arborized, acquiring dendritic-like and axonal-like identities, giving rise to a
416 variety of neuron-like morphologies. Furthermore, we have discovered a transient cell
417 nuclei lobulation coincident to *in vitro* neurogenesis, without being related to cell
418 proliferation. Cytokinesis, mitotic chromosomes and mitotic spindle were not observed
419 during the described of *in vitro* neurogenesis processes or neuronal polarization from
420 hPDLSCs. Moreover, the nuclear lamina and nucleolus are not disassembled during *in*
421 *vitro* neurogenesis from hPDLSCs.

422 Morphological analysis also revealed that the adult rodent V-SVZ of the anterolateral
423 ventricle wall, as well as the SGZ of the hippocampal dentate gyrus, where adult
424 neurogenesis has been clearly demonstrated, contains cells with nuclear shapes highly
425 similar to those observed during *in vitro* neurogenesis from hPDLSCs. Although it has
426 been suggested that lobed nuclei connected by an internuclear bridge are associated with
427 quiescence in aNSCs [20], we observed that this kind of nuclei is associated to nuclear
428 movement within the cell during initial phases of neurogenesis, without being related to
429 cell proliferation.

430 Taken together, these results suggest that the sequence of events from aNSCs to neuron
431 may also occur without being related to cell proliferation. It would therefore be interesting

432 to examine whether SVZ and SGZ intermediate progenitor cells represent different stages
433 of neurogenesis without being related to cell proliferation.

434 Furthermore, we demonstrate that hPDLSCs-derived neurons display a sequence of
435 morphologic development highly similar to those observed in primary neuronal cultures
436 derived from rodent brains during neurogenesis, providing strong evidence that it is
437 possible to reproduce neurogenic processes and obtain neurons from hPDLSCs, as
438 suggested by their neural-crest origin and stem cell characteristics [44]. The process of
439 neuronal polarization has been studied for decades using dissociated rodent embryonic
440 hippocampal pyramidal neurons and postnatal cerebellar granule neurons in culture [31,
441 32], but less is known about the process of neuronal polarization in human cells [37, 68].

442 Although future research is required to optimize the diversity of *in vitro* neural induction
443 protocols that have been designed for oral and dental stem cells [69], our results suggest
444 that hPDLSCs could also be used as an *in vitro* human cell-based model for neurogenesis
445 and neuronal polarization [37].

446 In addition, the easy procedure for obtaining these from adults in normal or pathological
447 conditions, may represent, as we have demonstrated with periodontal ligament cells
448 from children [70, 71], a suitable way of developing *in vitro* cell models of human
449 diseases.

450 Beyond the central nervous system, the presence of lobed nuclei has been reported in
451 most blood and immune cells, but the functional significance of multilobed nuclear
452 structures is not yet known [72-75]. We observed that multilobed nuclear structures is
453 associated to nuclear movement within the cell. It would also be interesting to examine
454 whether these putative mature cells also represent different stages of haematopoietic stem
455 cell differentiation without being related to cell proliferation. Thus, hPDLSCs could be

456 also used to understand the functional significance of multilobed nuclear structures in
457 blood and immune cells.

458 One of the most important discoveries in this work is the observation that small DNA
459 containing structures move within the cell to specific directions and temporarily form
460 lobed nuclei. These small DNA containing structures displayed a spherical or ovoid
461 shape, and it seems that some of them are connected to the main body of the nucleus by
462 thin strands of nuclear material. Fibrillarin and laminin A/C proteins were detected in
463 these small DNA containing structures.

464 It is known for many decades that chromatin particles can appear in the cellular cytoplasm
465 and they are referred to as micronuclei, nucleoplasmic bridge and nuclear bud [76].
466 Although these nuclear anomalies have been associated with chromosomal instability
467 events [76-79], recent reports showed generation of micronuclei during interphase [80-
468 82]. Therefore, the mechanisms that lead to extra-nuclear bodies formation and their
469 biological relevance are still far from been understood [83,84]. Ours results suggest that
470 the interphase cell nucleus can reversibly disassembled into functional subunits that
471 moved independently within the cell, if necessary.

472 In addition, alterations in nuclear morphologies are closely associated with a wide range
473 of human diseases, including muscular dystrophy and cancer [85,86]. Thus, hPDLSCs
474 could facilitate an understanding of the mechanisms regulating nuclear morphology in
475 response to cell shape changes and their functional relevance [87, 88].

476

477

478

479 5. Conclusions

480 Here, we show that hPDLSCs-derived neurons are not directly generated through cell
481 division from stem cells. In fact, the cell shape of neural precursors is reset and start their
482 neuronal development as round spheres. Futhermore, we have discovered a transient cell
483 nuclei lobulation coincident to *in vitro* neurogenesis, without being related to cell
484 proliferation. In addition, neurogenic niches in adult mouse brain contains cells with
485 nuclear shapes highly similar to those observed during *in vitro* neurogenesis from
486 hPDLSCs. Previous studies also show that the neurogenic niches in the adult mouse brain
487 and dissociated-cell cultures of hippocampal neurons contains cells with irregular nuclei
488 or even consist of two or more lobes connected by an internuclear bridge.

489 Taken together, these results suggest that the sequence of events from aNSCs to neuron
490 may also occur without being related to cell proliferation.

491 Futhermore, we demonstrate that hPDLSCs-derived neurons display a sequence of
492 morphologic development highly similar to those observed in primary neuronal cultures
493 derived from rodent brains during neurogenesis, providing strong evidence that it is
494 possible to reproduce neurogenic processes and obtain neurons from hPDLSCs.

495 The most important discovery in this work is the observation that small DNA containing
496 structures move within the cell to specific directions and temporarily form lobed nuclei.
497 Although the presence of lobed nuclei has been reported in most blood and immune cells,
498 and also in cancer cells, their functional significance remains elusive. Ours results suggest
499 that multilobed nuclear structures is associated to nuclear movement within the cell. Thus,
500 hPDLSCs could facilitate an understanding of the mechanisms regulating nuclear
501 morphology in response to cell shape changes and their functional relevance.

502

503 **Abbreviations:** aNSCs: Neural stem cells in the adult mammalian brain; hPDLSCs:
504 Human periodontal ligament stem cells; NSCs: Neural stem cells; V-SVZ: The
505 ventricular-subventricular zone; SGZ: subgranular zone; NCSCs; Neural crest stem cells;
506 PDL; periodontal ligament; Hpdl: human periodontal ligament.

507

508 **Declarations**

509 **Ethics approval and consent to participate:** Methods were carried out in accordance
510 with the relevant guidelines and regulations. The experimental protocols were approved
511 by the Institutional Review Board of the Miguel Hernández University of Elche (No.
512 UMH.IN.SM.03.16) and the signed informed consent was obtained from all patients
513 before the study. The authors declare that all experiments on human subjects were
514 conducted in accordance with the Declaration of Helsinki. All protocols and care of the
515 mice were carried out according to the guidelines of the European Community (Directive
516 86/609/ECC) and EU Directive 2010/63/EU for animal experiments in accordance with
517 the Society for Neuroscience recommendations.

518 **Consent for publication:** Not applicable.

519 **Availability of data and materials:** All data generated or analysed during this study are
520 included in this published article.

521 **Competing interest:** The authors declare that they have no competing interests.

522 **Funding:** This work was supported by the grants Institute of Health Carlos III
523 (RD16/001/0010) and Spanish MICINN (SAF2014-59347-C2-1-R) and (SAF2017-
524 83702-R).

525 **Authors' contributions:** CB conceived of the study, designed the study, carried out the
526 molecular lab work and drafted the manuscript. MM carried out the molecular lab work
527 and participated in data analysis. SM conceived of the study, helped draft the manuscript
528 and financial support. All authors read and approved the final manuscript.

529 **Acknowledgments:** We greatly appreciate the technical assistance of Microscopy
530 Section of the University of Murcia in preparing samples for scanning electron
531 microscopy.

532

533 **References**

534 1. Conti L, Cattaneo E. Neural stem cell systems: physiological players or in vitro
535 entities? *Nat Rev Neurosci.* 2010;11:176-187.

536 2. Doetsch F, Garcia-verdugo JM, Alvarez-buylla A. Cellular composition and three-
537 dimensional organization of the subventricular germinal zone in the adult mammalian
538 brain. *J Neurosci.* 1997;17:5046-61.

539 3. Doetsch F, Garcia-verdugo JM, Alvarez-buylla A. Regeneration of a germinal layer in
540 the adult mammalian brain. *Proc Natl Acad Sci.* 1999;96:11619-24.

541 4. Doetsch F, Caillé I, Garcia-verdugo JM, Alvarez-buylla A. Subventricular zone
542 astrocytes are neural stem cells in the adult mammalian brain. *Cell.* 1999;97:703-16.

543 5. Seri B, Garcia-verdugo, JM, McEwen BS, Alvarez-buylla A. Astrocytes give rise to
544 new neurons in the adult mammalian hippocampus. *J Neurosci.* 2001;21:7153-60.

545 6. Filippov V, Kronenberg G, Pivneva T, Reuter K, Steiner B, Wang LP, et al.
546 Subpopulation of nestin-expressing progenitor cells in the adult murine hippocampus

- 547 shows electrophysiological and morphological characteristics of astrocytes. *Mol Cell*
548 *Neurosci.* 2003;23:373-82.
- 549 7. Kronenberg G, Reuter K, Steiner B, Brandt MD, Jessberger S, Yamaguchi M, et al.
550 Subpopulations of proliferating cells of the adult hippocampus respond differently to
551 physiologic neurogenic stimuli. *J Comp Neurol.* 2003;467:455-63.
- 552 8. Seri B, Garcia-verdugo JM, Collado-Morente L, McEwen BS, Alvarez-buylla A. Cell
553 types, lineage, and architecture of the germinal zone in the adult dentate gyrus. *J Com*
554 *Neurol.* 2004;474:359-78.
- 555 9. Kempermann G, Jessberger S, Steiner B, Kronenberg G. Milestones of neuronal
556 development in the adult hippocampus. *Trends Neurosci.* 2004;27:447-52.
- 557 10. Bond AM, Ming GL, Song H. Adult mammalian neural stem cells and neurogenesis:
558 five decades later. *Cell Stem Cell.* 2015;17:385-95.
- 559 11. Fuentealba LC, Obernier K, Alvarez-Buylla A. Adult stem cells bridge their niche.
560 *Cell Stem Cell.* 2012;10:678-708.
- 561 12. Reynolds BA, Weiss S. Generation of neurons and astrocytes from isolated cells of
562 the adult mammalian central nervous system. *Science.* 1992;255:1707-10.
- 563 13. Gabay L, Lowell S, Rubin LL, Anderson DJ. Deregulation of dorsoventral patterning
564 by FGF confers trilineage differentiation capacity on CNS stem cells in vitro. *Neuron.*
565 2003;40:485-99.
- 566 14. Suh H, Consiglio A, Ray J, Sawai T, D'Amour KA, Gage FH. In vivo fate analysis
567 reveals the multipotent and self-renewal capacities of Sox2⁺ neural stem cells in the adult
568 hippocampus. *Cell Stem Cell.* 2007;1:515-28.

- 569 15. Smart I. The subependymal layer of the mouse brain and its cell production as shown
570 by radioautography after thymidine-H3 injection. *J Com Neurol.* 1961;116:325-47.
- 571 16. Privat A, Leblond CP. The subependymal layer and neighboring region in the brain
572 of the young rat. *J Com Neurol.* 1972;146:277-302.
- 573 17. Sturrock RR, Smart IH. A morphological study of the mouse subependymal layer
574 from embryonic life to old age. *J Anat Mar.* 1980;130:391-415.
- 575 18. Guerrero-Cázares H, Gonzalez-Perez O, Soriano-Navarro M, Zamora-Berridi G,
576 García-Verdugo, JM, Quinoñes-Hinojosa A. Cytoarchitecture of the lateral ganglionic
577 eminence and rostral extension of the lateral ventricle in the human fetal brain. *J Comp*
578 *Neurol.* 2011;519:1165-80.
- 579 19. Capilla-Gonzalez V, Cebrian-Silla A, Guerrero-Cazares H, Garcia-Verdugo JM,
580 Quiñones-Hinojosa A. Age-related changes in astrocytic and ependymal cells of the
581 subventricular zone. *Glia.* 2014;62:790-803.
- 582 20. Cebrián-Silla A, Alfaro-Cervelló C, Herranz-Pérez V, Kaneko N, Park DH,
583 Sawamoto K, et al. Unique organization of the nuclear envelope in the post-natal
584 quiescent neural stem cells. *Stem Cell Reports.* 2017;9:203-216.
- 585 21. Ribak CE, Anderson L. Ultrastructure of the pyramidal basket cells in the dentate
586 gyrus of the rat. *J Comp Neurol.* 1980;192:903-916.
- 587 22. Ribak CE, Seress L. Five types of basket cell in the hippocampal dentate gyrus: a
588 combined Golgi and electron microscopic study. *J Neurocytol.* 1983;12:577-97.
- 589 23. Kaplan MS, Bell DH. Mitotic neuroblasts in the 9-day-old and 11-month-old rodent
590 hippocampus. *J Neurosci.* 1984;4:1429-41.

- 591 24. Seress L, Ribak CE. A combined Golgi-electron microscopic study of non-pyramidal
592 neurons in the CA 1 area of the hippocampus. *J Neurocytol.* 1985;14:717-30.
- 593 25. Seki T, Arai Y. Highly polysialylated neural cell adhesion molecule (NCAM-H) is
594 expressed by newly generated granule cells in the dentate gyrus of the adult rat. *J*
595 *Neurosci.* 1993;13:2351-58.
- 596 26. Kuhn HG, Dickinson-Anson H, Gage FH. Neurogenesis in the dentate gyrus of the
597 adult rat: Age-Related decrease of neuronal progenitor proliferation. *J Neurosci.* 1996;16:
598 2027-33.
- 599 27. Parent JM, Yu TW, Leibowitz RT, Geschwind DH, Sloviter RS, Lowenstein DH.
600 Dentate granule cell neurogenesis is increased by seizures and contributes to aberrant
601 network reorganization in the adult rat hippocampus. *J Neurosci.* 1997;17:3727-38.
- 602 28. Urbach A, Redecker C, Witte OW. Induction of neurogenesis in the adult dentate
603 gyrus by cortical spreading depression. *Stroke.* 2008;39:3064-72.
- 604 29. Wittmann M, Queisser G, Eder A, Wiegert JS, Bengtson CP, Hellwig A, et al.
605 Synaptic activity induces dramatic changes in the geometry of the cell nucleus: interplay
606 between nuclear structure, histone H3 phosphorylation, and nuclear calcium signaling. *J*
607 *Neurosci.* 2009;29:14687-700.
- 608 30. Ghashghaei HT, Lai C, Anton ES. Neuronal migration in the adult brain: are we there
609 yet? *Nat Rev Neurosci.* 2007;8:141-51.
- 610 31. Tahirovic S, Bradke F. Neuronal polarity. *Cold Spring Harb Perspect Biol.* 2009;doi:
611 10.1101/cshperspect.a001644
- 612 32. Takano T, Xu C, Funahashi Y, Namba T, Kaibuchi K. Neuronal polarization.
613 *Development.* 2015;142:2088-93.

- 614 33. Dotti CG, Sullivan CA, Banker GA. The establishment of polarity by hippocampal
615 neurons in culture. *J Neurosci.* 1988;8:1454-68.
- 616 34. Powell SK, Rivas RJ, Rodriguez-Boulan E, Hatten ME. Development of polarity in
617 cerebellar granule neurons. *J Neurobiol.* 1997;32:223-36.
- 618 35. Casarosa, S, Bozzi Y, Conti L. Neural stem cells: ready for therapeutic applications?
619 *Mol Cell Ther.* 2014;2:31.
- 620 36. Goldman SA. Stem and progenitor cell-based therapy of the central nervous system:
621 hopes, hype, and wishful thinking. *Cell Stem Cell.* 2016;18:174-88.
- 622 37. Azari H, Reynolds BA. In vitro models for neurogenesis. *Cold Spring Harbour*
623 *Perspectives in Biology.* 2016; doi: 10.1101/cshperspect.a021279.
- 624 38. Bronner-Fraser M. Origins and developmental potential of the neural crest. *Exp Cell*
625 *Res.* 1995;218:405-17.
- 626 39. Crane JF, Trainor PA. Neural crest stem and progenitor cells. *Annu Rev Cell Dev*
627 *Biol.* 2016;22:267–86.
- 628 40. Achilleos A, Trainor, PA. Neural crest stem cells: discovery, properties and potential
629 for therapy. *Cell Res.* 2012;22:288-304.
- 630 41. Liu JA, Cheung M. Neural crest stem cell and their potential therapeutic applications.
631 *Dev Biol.* 2016;419:199-216.
- 632 42. Seo BM, Miura M, Gronthos S, Bartold PM, Batouli S, Brahim J, et al. Investigation
633 of multipotent postnatal stem cells from human periodontal ligament. *Lancet.*
634 2004;364:149–155.

- 635 43. Tomokiyo A, Yoshida S, Hamano S, Hasegawa D, Sugii H, Maeda H. Detection,
636 Characterization, and Clinical Application of Mesenchymal Stem Cells in Periodontal
637 Ligament Tissue. *Stem Cells Int.* 2018; doi: 10.1155/2018/5450768.
- 638 44. Bueno C, Ramirez C, Rodríguez-Lozano FJ, Tabarés-Seisdedos R, Rodenas M,
639 Moraleda JM, et al. Human adult periodontal ligament-derived cells integrate and
640 differentiate after implantation into the adult mammalian brain. *Cell Transplant.* 2013;22:
641 2017-28.
- 642 45. Fortino VR, Chen RS, Pelaez D, Cheung HS. Neurogenesis of neural crest-derived
643 periodontal ligament stem cells by EGF and bFGF. *J Cell Physiol.* 2014;229:479-88.
- 644 46. Ng TK, Yung JS, Choy KW, Cao D, Leung CK, Cheung HS, Pang CP.
645 Transdifferentiation of periodontal ligament-derived stem cells into retinal ganglion-like
646 cells and its microRNA signature. *Sci Rep.* 2015; doi: 10.1038/srep16429.
- 647 47. Flynn KC. The cytoskeleton and neurite initiation. *BioArchitecture.* 2013;3:86-109.
- 648 48. Foudah D, Monfrini M, Donzelli E, Niada S, Brini AT, Orciani M, et al. Expression
649 of neural markers by undifferentiated mesenchymal-like stem cells from different
650 sources. *J Immunol Res.* 2014; doi: 10.1155/2014/987678.
- 651 49. Jouhilahti EM, Peltonen S, Peltonen J. Class III beta-tubulin is a component of the
652 mitotic spindle in multiple cell types. *J Histochem Cytochem.* 2008;56:1113-19.
- 653 50. Forscher P, Smith SJ. Actions of Cytochalasins on the organization of actin filaments
654 and microtubules in a neuronal growth cone. *J Cell Biol.* 1988;107:1505-16.
- 655 51. Blanquie O, Bradke F. Cytoskeleton dynamics in axon regeneration. *Curr Opin*
656 *Neurobiol.* 2018;51:60-69.

- 657 52. Ros O, Cotrufo T, Martinez-Marmol R, Soriano E. Regulation of patterned Dynamics
658 of local exocytosis in growth cone by netrin-1. *J Neurosci*. 2015;35:5156-70.
- 659 53. Hering H, Sheng M. Dendritic spines: Structure, dynamics and regulation. *Nature Rev*
660 *Neurosci*. 2001;2:880-88.
- 661 54. Von Bohlen Und Halbach O. Structure and functions of dendritic spines. *Ann Anat*.
662 2009;191:518-31.
- 663 55. Merriam EB, Millette M, Lumbard DC, Saengsawang W, Fothergill T, Hu X, et al.
664 Synaptic regulation of microtubule dynamics in dendritic spines by calcium, F-actin, and
665 debrin. *J Neurosci*. 2013;33:164711-82.
- 666 56. Gibson DA, Ma L. Developmental regulation of axon branching in the vertebrate
667 nervous system. *Development*. 2011;138:183-195.
- 668 57. Ochs RL, Lischwe MA, Spohn WH, Busch H. Fibrillarin: a new protein of the
669 nucleolus identified by autoimmune sera. *Biol Cell*. 1985;54:123-33.
- 670 58. De Leeuw R, Gruenbaum Y, Medalia O. Nuclear Lamins: Thin Filaments with Major
671 Functions. *Trends Cell Biol*. 2018;28:34-45.
- 672 59. Rodriguez-Corona U, Sobol M, Rodriguez-Zapata LC, Hozak P, Castano E.
673 Fibrillarin from Archaea to human. *Biol Cell*. 2015;107:159-74.
- 674 60. Németh A, Grummt I. Dynamic regulation of nucleolar architecture. *Curr Opin Cell*
675 *Biol*. 2018;52:105-11.
- 676 61. Cooper-Kuhn CM, Kuhn HG. Is it all DNA repair? Methodological considerations
677 for detecting neurogenesis in the adult brain. *Brain Res Dev Brain Res*. 2002;134:13-21.

- 678 62. Sohur US, Emsley JG, Mitchell BD, Macklis JD. Adult neurogenesis and cellular
679 brain repair with neural progenitors, precursors and stem cells. *Philos Trans R Soc Lond*
680 *B Biol Sci.* 2006;361:1477-97.
- 681 63. Kuhn HG, Eisch AJ, Spalding K, Peterson DA. Detection and Phenotypic
682 Characterization of Adult Neurogenesis. *Cold Spring Harb Perspect. Biol.* 2016; doi:
683 10.1101/cshperspect.a025981.
- 684 64. Cameron HA, Woolley CS, McEwen BS, Gould E. Differentiation of newly born
685 neurons and glia in the dentate gyrus of the adult rat. *Neuroscience.* 1993;56:337-44.
- 686 65. Palmer TD, Ray J, Gage FH. FGF-2-responsive neuronal progenitors reside in
687 proliferative and quiescent regions of the adult rodent brain. *Mol Cell Neurosci.* 1995;6:
688 474-86.
- 689 66. Uberti D, Ferrar-Toninelli G, Memo M. Involvement of DNA damage and repair
690 systems in neurodegenerative process. *Oxico l Lett.* 2003;139:99-105.
- 691 67. Van Oijen MG, Medema RH, Slootweg PJ, Rijksen G. Positivity of the proliferation
692 marker Ki-67 in noncycling cells. *Am J Clin Pathol.* 1998;110:24-31.
- 693 68. Ohara Y, Koganezawa N, Yamazaki H, Roppongi RT, Sato K, Sekino Y, Shirao T.
694 Early-stage development of human induced pluripotent stem cell-derived neurons. *J*
695 *Neurosci Res.* 2015;93:1804-13.
- 696 69. Heng BC, Lim LW, Wu W, Zhang C. An Overview of Protocols for the Neural
697 Induction of Dental and Oral Stem Cells In Vitro. *Tissue Eng Part B Rev.* 2016;22:220-
698 50.

- 699 70. Jones J, Estirado A, Redondo C, Bueno C, Martínez S. Human adipose stem cell-
700 conditioned médium increases survival of friedreich`s ataxia cells submitted to oxidative
701 stress. *Stem Cells Dev.* 2012;21:2817-26.
- 702 71. Quesada MP, Jones J, Rodríguez-Lozano FJ, Moraleda JM, Martinez S. Novel
703 aberrant genetic and epigenetic events in friedreich`s ataxia. *Exp Cell Res.* 2015;335:51-
704 61.
- 705 72. Hoffmann K, Sperling K, Olins AL, Olins DE. The granulocyte nucleus and lamin B
706 receptor: avoiding the ovoid. *Chromosoma.* 2007;116:227-35.
- 707 73. Carvalho LO, Aquino EN, Neves AC, Fontes W. The neutrophil nucleus and its role
708 in neutrophilic function. *J Cell Biochem.* 2015;116:1831-36.
- 709 74. Skinner BM, Johnson EE. Nuclear morphologies: their diversity and functional
710 relevance. *Chromosoma.* 2017;126:195-212.
- 711 75. Georgopoulos K. In search of the mechanism that shapes the neutrophil`s nucleus
712 *Genes Dev.* 2017;31:85-87.
- 713 76. Fenech M, Kirsch-Volders M, Natarajan AT, Surralles J, Crott JW, Parry J, et al.
714 Molecular mechanisms of micronucleus, nucleoplasmic bridge and nuclear bud formation
715 in mammalian and human cells. *Mutagenesis.* 2011;26:125-32.
- 716 77. Hutchison HE, Ferguson-Smith MA. The significance of Howell-Jolly bodies in red
717 cell precursors. *J Clin Pathol.* 1959;12:451-53
- 718 78. Dawson DW, Bury HP. The significance of Howell-Jolly bodies and giant
719 metamyelocytes in marrow smears. *J Clin Pathol.* 1961;14:374-80.

- 720 79. Heddle JA, Carrano AV. The DNA content of micronuclei induced in mouse bone
721 marrow by gamma-irradiation: evidence that micronuclei arise from acentric
722 chromosomal fragments. *Mutat Res.* 1977;44:63-69.
- 723 80. Shimizu N, Itoh N, Utiyama H, Wahl GM. Selective entrapment of
724 extrachromosomally amplified DNA by nuclear budding and micronucleation during S
725 phase. *J Cell Biol.* 1998;140:1307-20.
- 726 81. Haaf T, Raderschall E, Reddy G, Ward DC, Radding CM, Golub EI. Sequestration of
727 mammalian Rad51-recombination protein into micronuclei. *J Cell Biol.* 1999;144:11-20.
- 728 82. Utani K, Okamoto A, Shimizu N. Generation of micronuclei during interphase by
729 coupling between cytoplasmic membrane blebbing and nuclear budding. *PLoS One.*
730 2011; doi: 10.1371/journal.pone.0027233.
- 731 83. Hintzsche H, Hemmann U, Poth A, Utesch D, Lott J, Stopper H. Fate of micronuclei
732 and micronucleated cells. *Mutat Res.* 2017;771:85-98.
- 733 84. Norppa H, Falck GC. What do human micronuclei contain? *Mutagenesis.*
734 2003;18:221-33.
- 735 85. Zink D, Fischer AH, Nickerson JA. Nuclear structure in cancer cells. *Nat Rev Cancer.*
736 2004;4:677-87.
- 737 86. Gundersen GG, Worman HJ. Nuclear positioning. *Cell.* 2013;152:1376-89.
- 738 87. Dupin I, Etienne-Manneville S. Nuclear positioning: mechanisms and functions. *Int J*
739 *Biochem Cell Biol.* 2011;43:1698-707.
- 740 88. Skinner BM, Johnson EE. Nuclear morphologies: their diversity and functional
741 relevance. *Chromosoma.* 2017;126:195-212.

742 **Figure legends**

743 **Fig. 1. Morphological changes in hPDLSCs cultures during neural induction.**

744 Undifferentiated hPDLSCs presented a fibroblast-like morphology with low-density
745 microvilli on their surface (a) and actin microfilaments and β -III tubulin microtubules
746 oriented parallel to the longitudinal axis of the cell (b). (c) Western blot analysis verified
747 the expression of β -III tubulin. Protein size markers (in kilodaltons) are indicated on the
748 side of the panel. (d) During mitosis, β -III tubulin is present in the mitotic spindle and it
749 is detectable in all phases of mitosis. (e) Undifferentiated hPDLSCs displayed a flattened,
750 ellipsoidal nucleus often located in the center of the cell. (f) After 14 days of neural
751 differentiation conditions, hPDLSCs with different morphologies were observed. (g) In
752 addition, hPDLSCs of various size were also observed. (h) Microscopic analysis also
753 revealed that some hPDLSCs have different nuclear size and shapes, including lobed
754 nuclei connected by an internuclear bridge. Scale bar: 25 μ m. SEM, scanning electron
755 microscopy; LM, light microscopy.

756 **Fig. 2. *In vitro* neurogenesis from hPDLSCs.**

757 (a) After neural induction, hPDLSCs undergo a shape and size change, adopting highly
758 irregular forms first and then gradually contracting into round cells. (b) Cytoskeletal
759 remodeling is observed during these morphological changes. Actin microfilament not
760 longer surround the nucleus and become cortical. Unlike actin, β -III tubulin seems to
761 accumulate around the nucleus. (c) the cytoskeletal network is almost lost in round cells.
762 (d) Scanning electron micrographs show that there is a marked increase in the density of
763 microvilli as the cells round up to near-spherical shape. (e) The surface of round cells is
764 almost devoid of microvilli. The scale bars are 25 μ m in the light microscope images, and

765 10 μm in the scanning electron micrographs. LM, light microscopy; SEM, scanning
766 electron microscopy.

767 **Fig. 3. Neuronal polarization of hPDLSCs-derived neurons.**

768 (a) hPDLSCs-derived neurons start their development as rounded spheres that initiate
769 neurite outgrowth at a single site on the plasma membrane. (b) These later transform into
770 cells containing several short neurites developed around the cell body. (c) the cytoskeletal
771 network is reorganized. β -III tubulin accumulates densely under the cellular membrane
772 of the cell body and in cell neurites while actin microfilaments are mainly found in cell
773 neurites. (d) The peripheral domain in the growth cone of hPDLSCs-derived neurons is
774 composed of radial F-actin bundles and the central domain contains β -III tubulin
775 microtubules. (e) Micrographs showing that the growth cone also contains filopodia and
776 vesicles on the cell surface. At later stages of development, hPDLSCs-derived neurons
777 gradually adopt a complex morphology (f) giving rise to a variety of neuron-like forms
778 (g). (h) Cytoskeletal protein β -III tubulin and F-actin staining shown that hPDLSCs-
779 derived neurons develop distinct axon-like and dendrite-like processes (numbers locate
780 the areas shown in higher power). The scale bars are 25 μm in the light microscope
781 images, and 10 μm in the scanning electron micrographs. SEM, scanning electron
782 microscopy; LM, light microscopy; b, actin bundles; v, vesicles, f, filopodia.

783 **Fig. 4. hPDLSCs-derived neurons have developed well-differentiated axonal-like**
784 **and dendritic-like domains.**

785 (a) Scanning electron micrographs show that hPDLSCs-derived neurons are composed of
786 multiple branched processes with different spine-like protusions highly similar to
787 filopodium, mushroom, thin, stubby, and branched dendritic spines shapes. hPDLSCs-
788 derived neurons also display different types of axonal branch-like structures, including

789 bifurcation (b), terminal arborization (c), and collateral formation (d) (inserts and
790 numbers locate the areas showed in higher power). The scale bars are 25 μm in light
791 microscope images and 5 μm in the scanning electron micrographs. SEM, scanning
792 electron microscopy; LM, light microscopy; s, spine-like protusions; f, filopodium; m,
793 mushroom; t, thin; stubby; b, branched. B, bifurcation; a, arborization; c, collateral
794 formation.

795 **Fig. 5. hPDLSCs-derived neurons are connected by synapse-like interactions.**

796 hPDLSCs-derived neurons connect to one another (a) through different types of
797 synapses-like interactions, including dendrodendritic-like, axoaxonic-like and
798 axodendritic-like synapses (b). (c) Synapse-associated proteins Cx43, Synaptophysin and
799 Synapsin1 are found in the cell membrane of hPDLSCs-derived neurons at the neurite
800 contact areas. Scale bar: 25 μm . LM, light microscopy; DD, dendrodendritic-like synapse;
801 AA, axoaxonic-like and synapse; AD, axodendritic-like synapse.

802 **Fig. 6. Dynamic localization of fibrillarin and laminin A/C proteins during the cell**
803 **cycle of hPDLSCs.**

804 (a) During interphase, the nuclei of hPDLSCs contained two or more nucleoli and the
805 inside surface of the nuclear envelope is lined with the nuclear lamina. (b) The nuclear
806 lamina and nucleolus are reversibly disassembled during mitosis. Scale bar: 10 μm .

807 **Fig. 7. Nuclear shape remodeling occurs during neurogenesis from hPDLSCs.**

808 (a,n) Small DNA containing structures start to move towards specific positions within the
809 cell and temporarily form lobed nuclei (o,r). Later, these lobed nuclei connected to one
810 another through small structures containing DNA (s,x) forming internuclear bridges (y,z).
811 Scale bar: 10 μm .

812 **Fig. 8. Nuclear shape remodeling occurs during neurogenesis from hPDLSCs.**

813 (a,j) lobed nuclei connected by internuclear bridges move towards specific positions
814 within the cell and finally, there is restoration of irregular, but non-lobed, nucleus with an
815 eccentric position within hPDLSCs-derived neurons (k,o). The scale bars in β -III tubulin
816 and DAPI images are 50 μ m and 10 μ m for confocal 3D images of nuclei.

817 **Fig. 9. Cytoplasmic DNA containing structures.**

818 (a) Cytoplasmic DNA containing structures displayed a spherical or ovoid shape and it
819 seems that some of them are connected to the main body of the nucleus by thin strands of
820 nuclear material (b). Scale bar: 5 μ m.

821 **Fig. 10. Dynamic localization of fibrillarin and laminin A/C proteins during**
822 **neurogenesis from hPDLSCs**

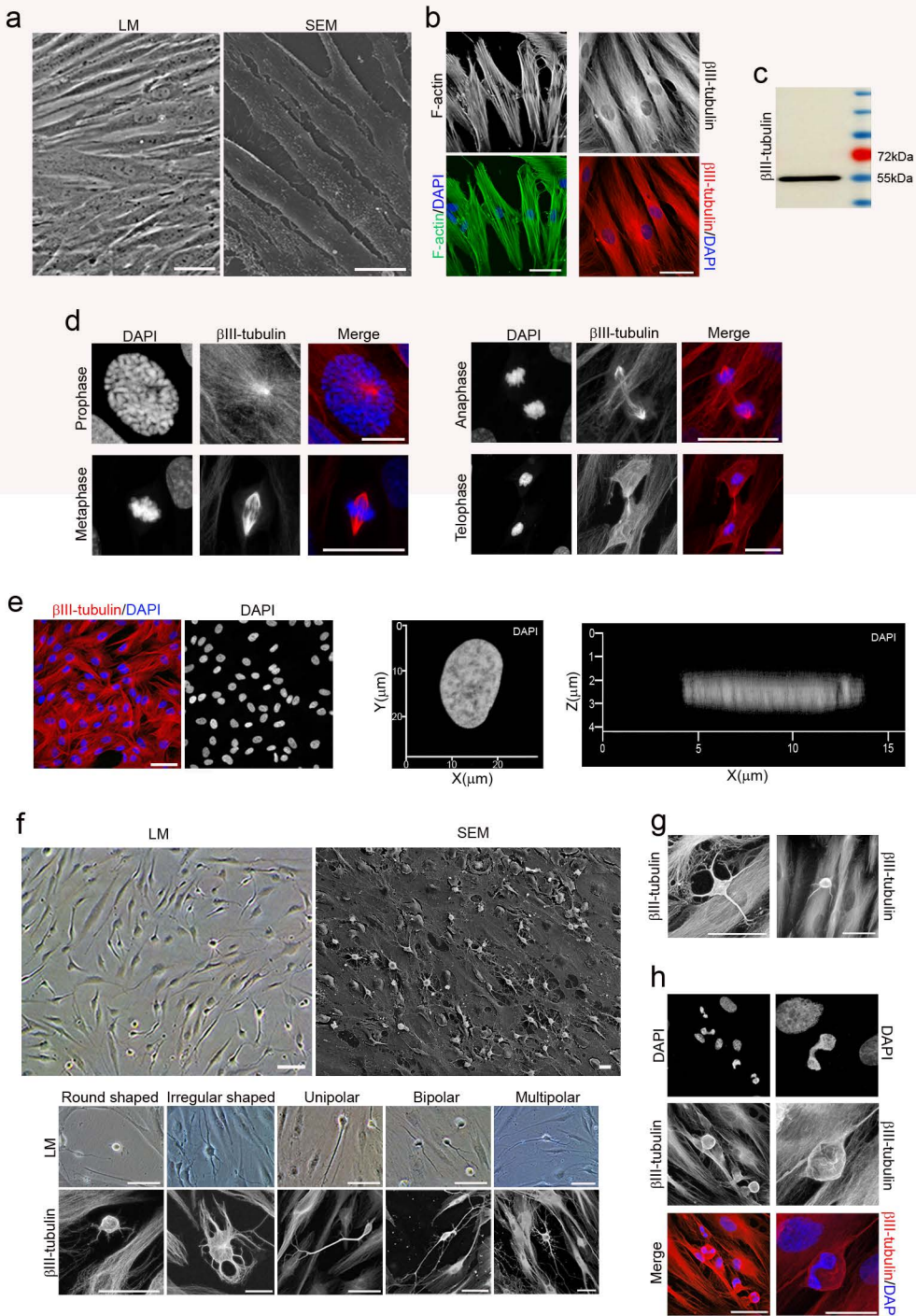
823 (a) Fibrillarin and laminin A/C proteins were detected in small DNA containing structures
824 (numbers locate the areas showed in higher power). (b) The nuclear lamina and nucleolus
825 are not disassembled during *in vitro* neurogenesis from hPDLSCs. Scale bar: 5 μ m.

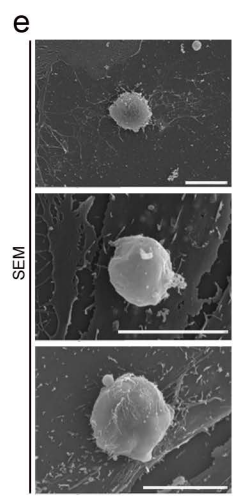
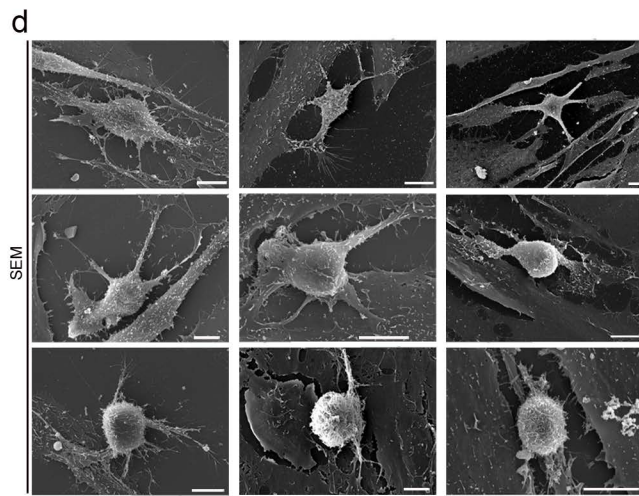
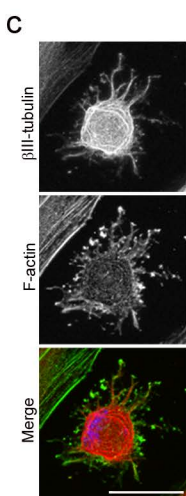
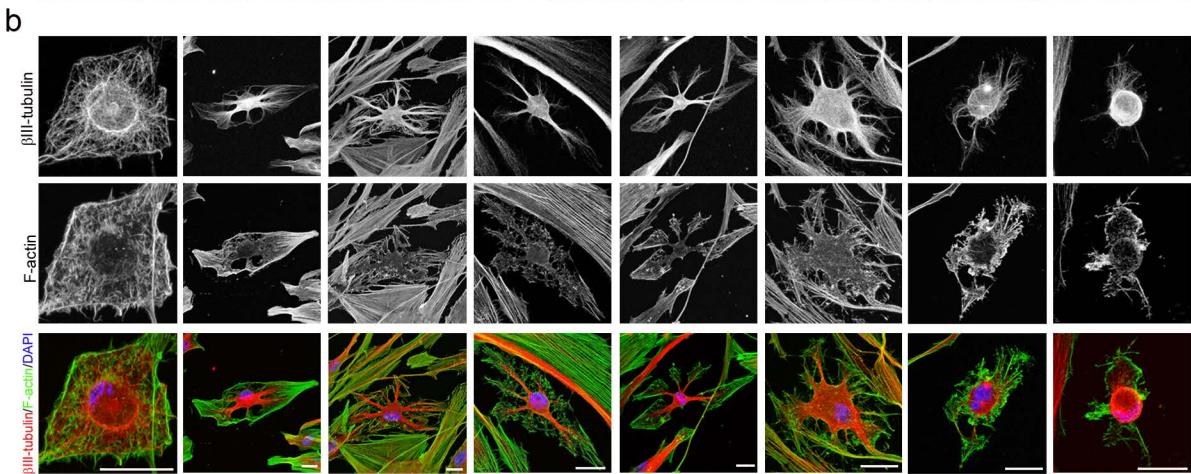
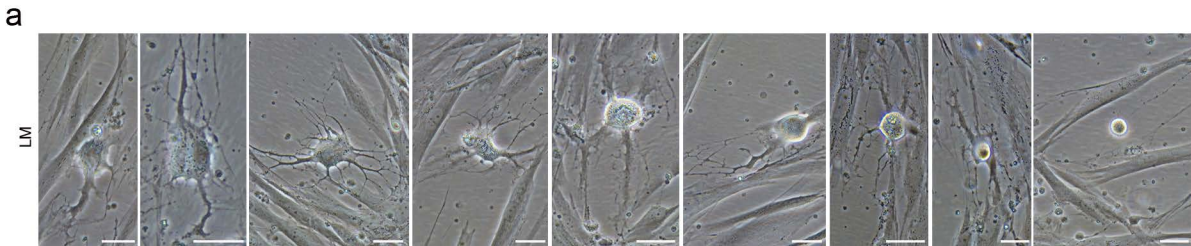
826 **Fig. 11. Nuclear shape in PDL-derived neurons.**

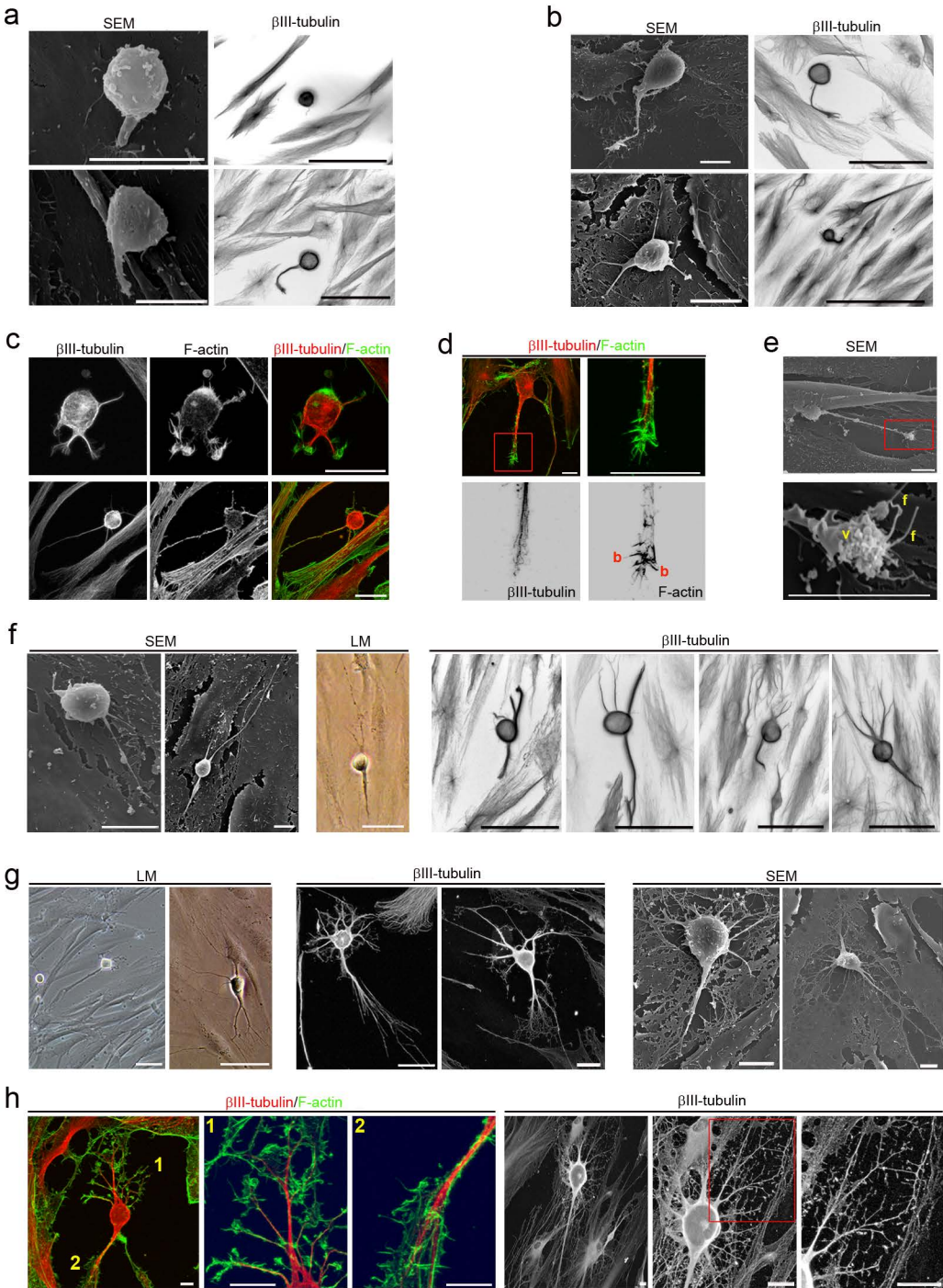
827 (a) No lobed nuclei are observed when PDL-derived neurons gradually acquired cellular
828 polarity and more mature, neuronal-like morphology. (b) The nuclear volume shrinks as
829 the cells become rounded during neurogenesis. Data represent mean \pm S.E. of ten
830 independent experiments. The scale bar in β -III tubulin and DAPI images are 50 μ m and
831 10 μ m for confocal 3D images of nuclei.

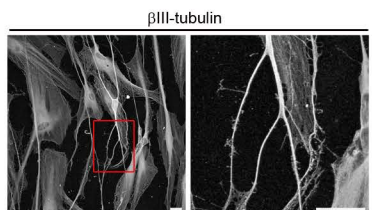
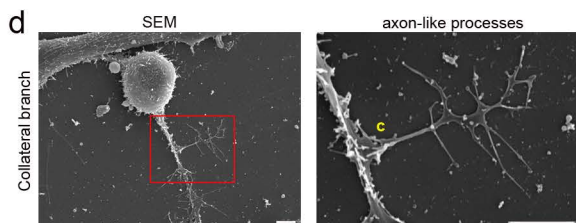
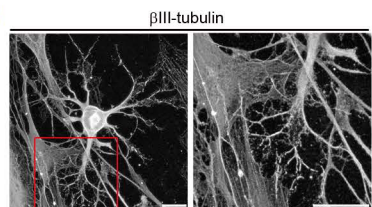
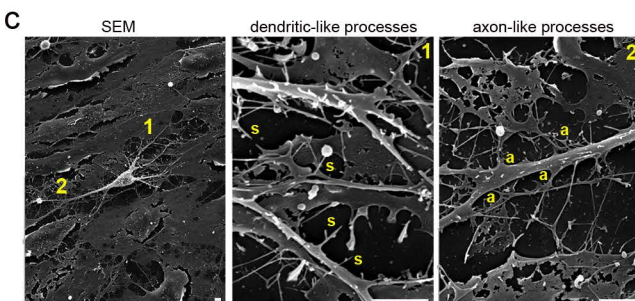
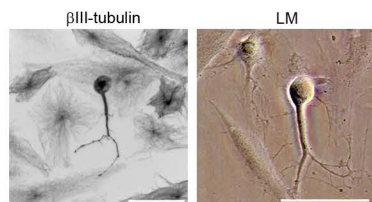
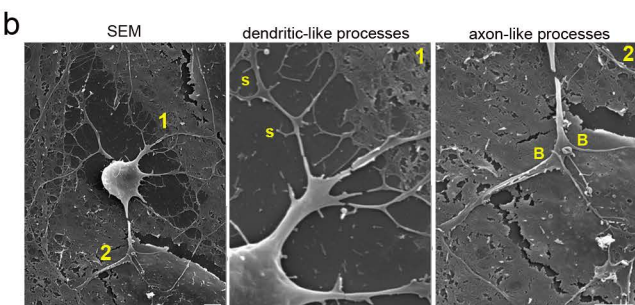
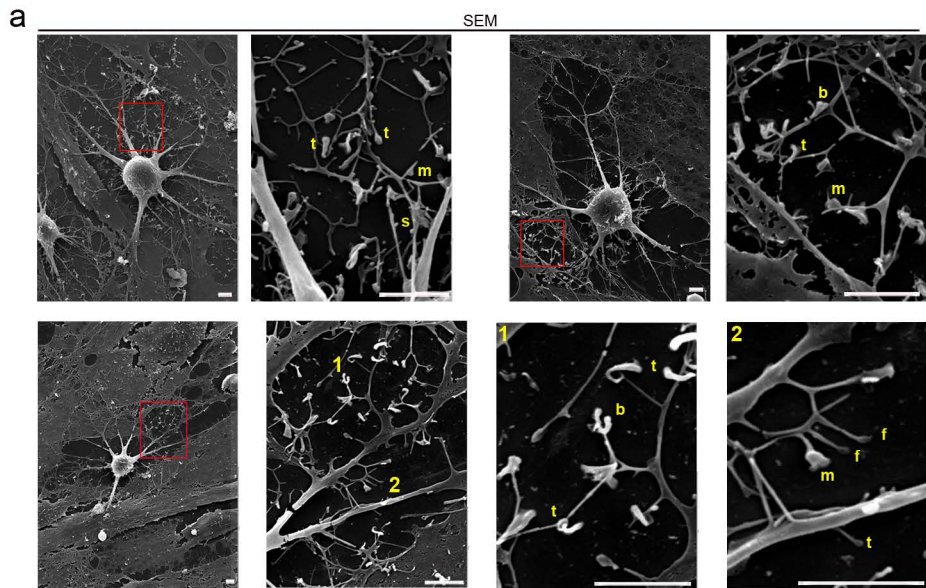
832 **Fig. 12. Neurogenic niches in the adult mammalian brain also contains cells with**
833 **irregular nuclei.** Morphological analysis reveals that the adult rodent V-SVZ of the
834 anterolateral ventricle wall (a), as well as the SGZ of the hippocampal dentate gyrus (b),

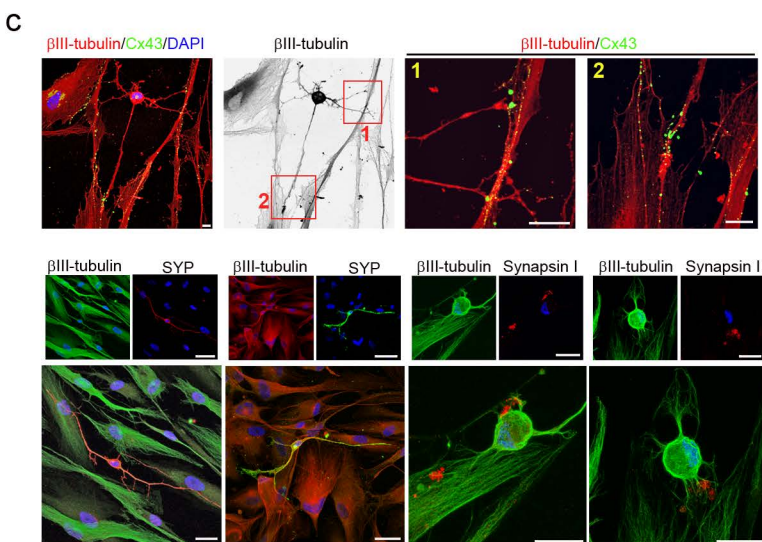
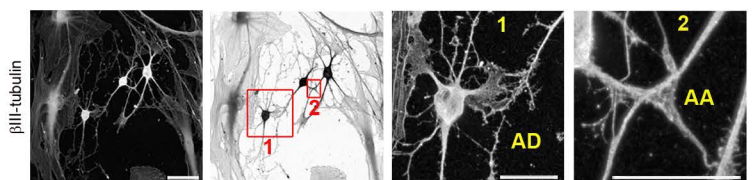
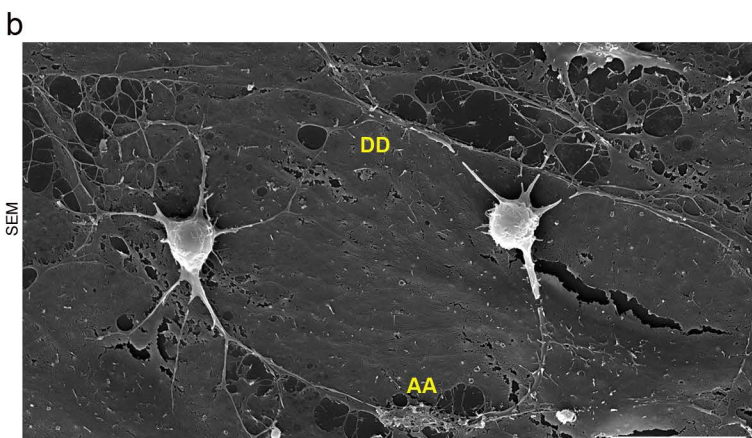
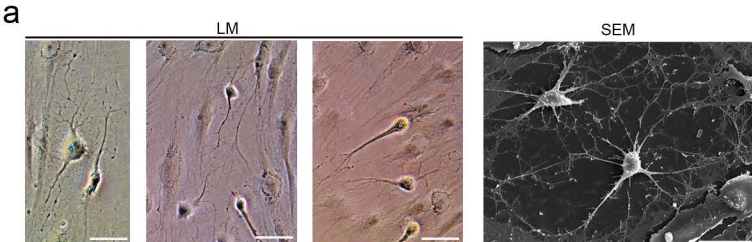
835 contain cells with nuclear shapes highly similar to those observed in during *in vitro*
836 neurogenesis from hPDLSCs. Scale bar: 10 μ m. LV, lateral ventricle; GLC, granule cell
837 layer.

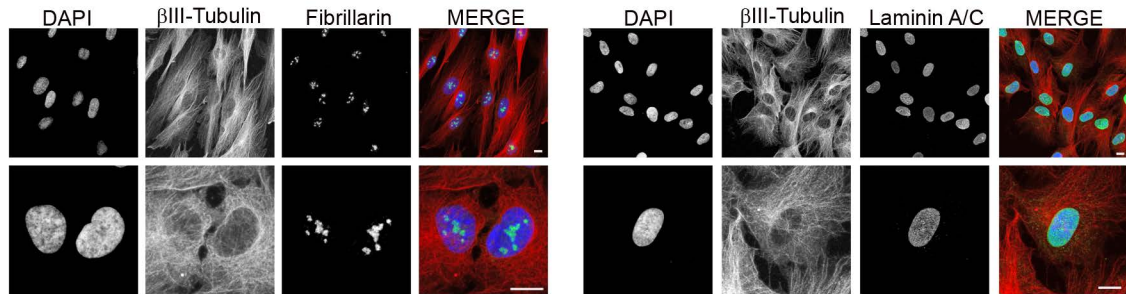
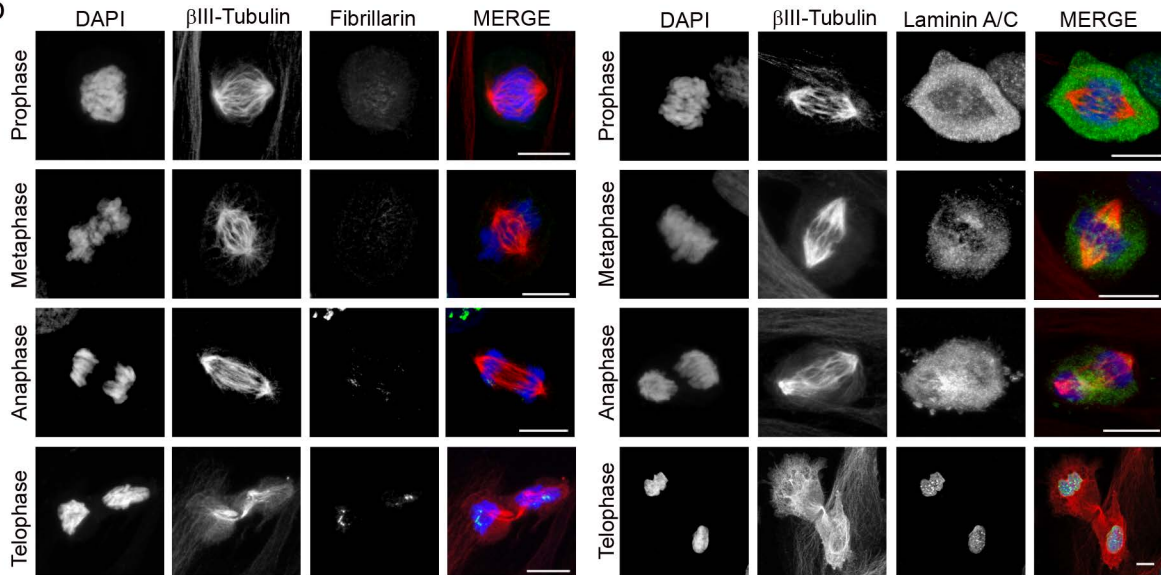


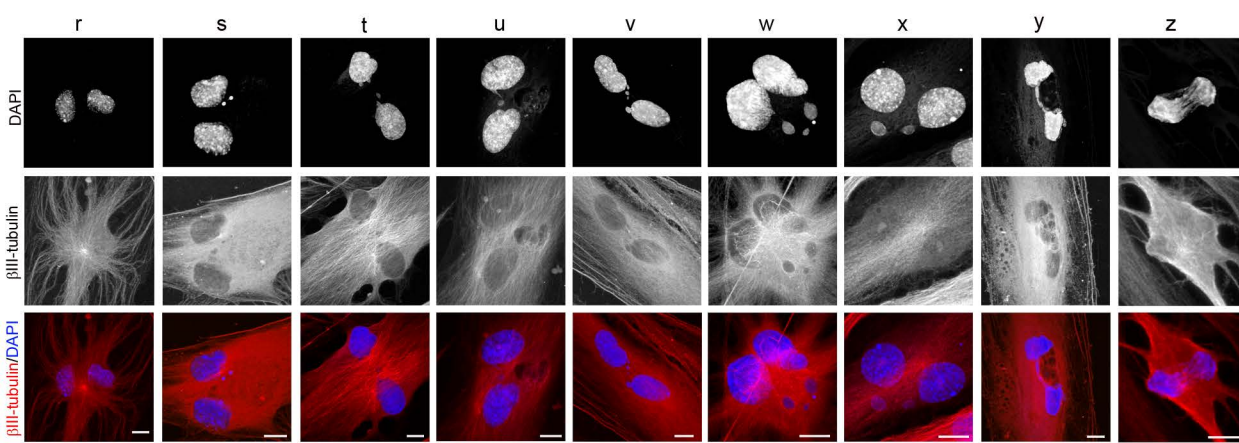
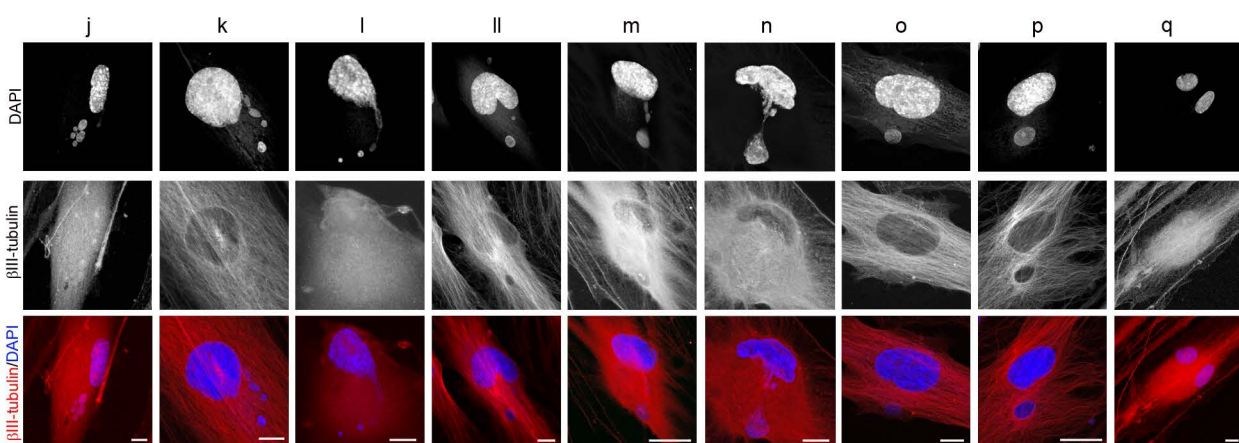
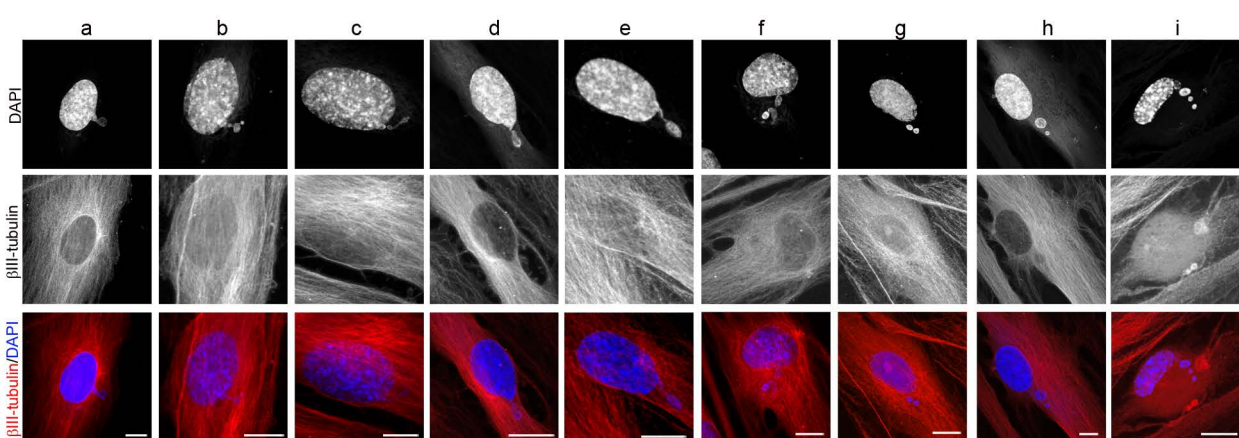


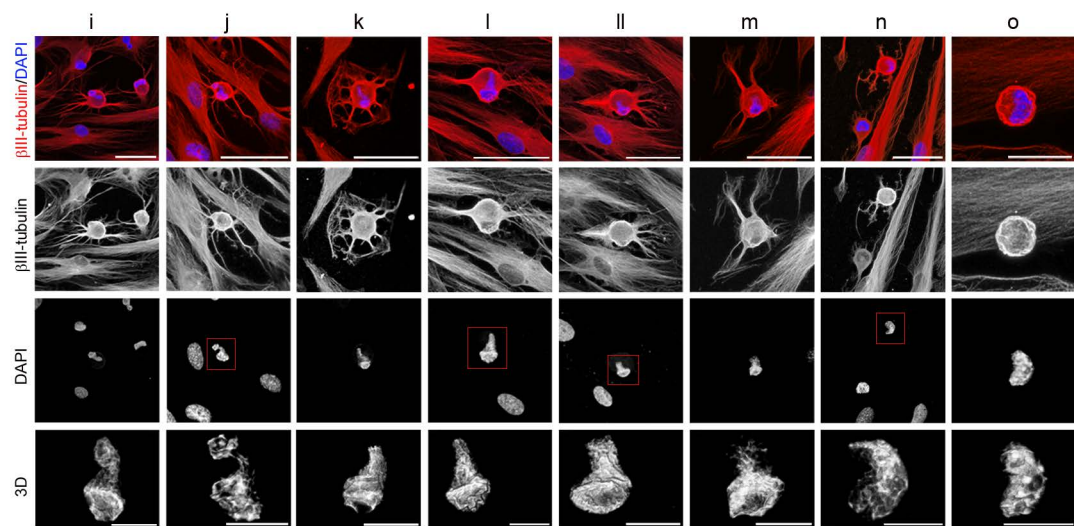
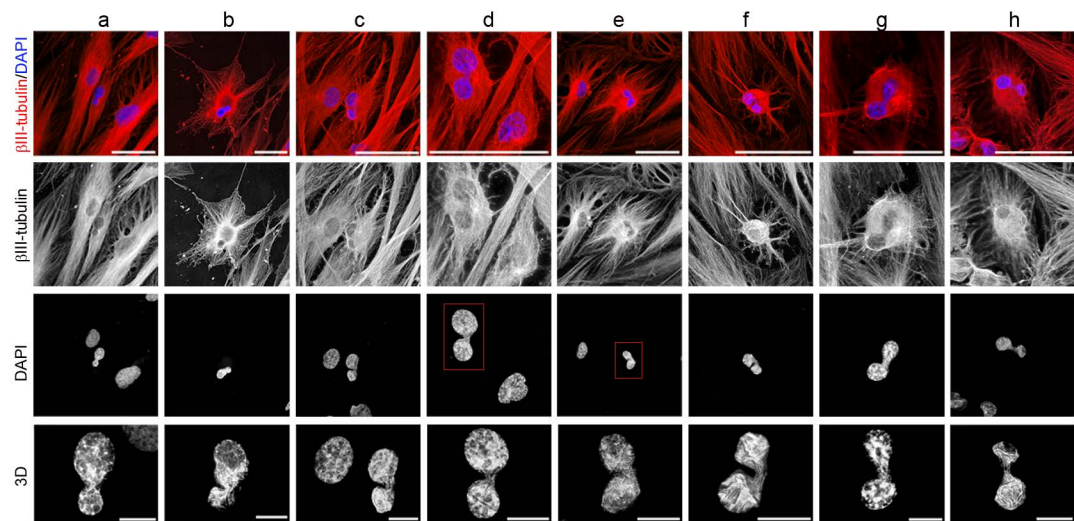


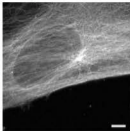
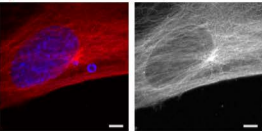
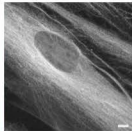
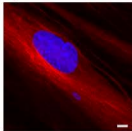
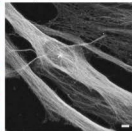
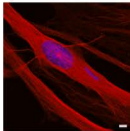
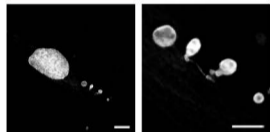
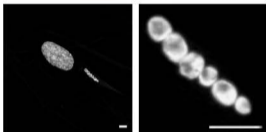
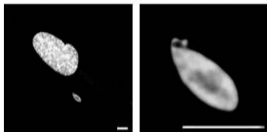
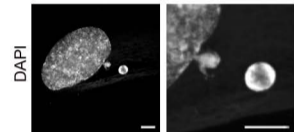
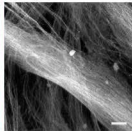
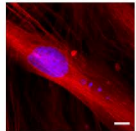
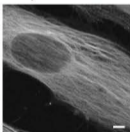
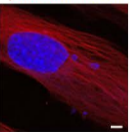
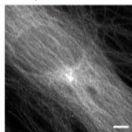
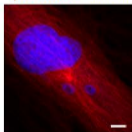
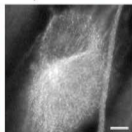
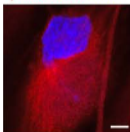
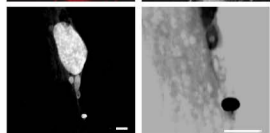
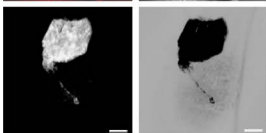
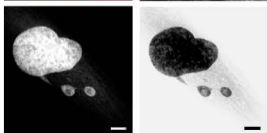
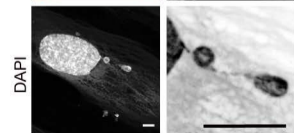
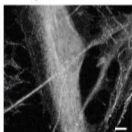
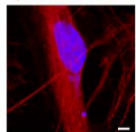


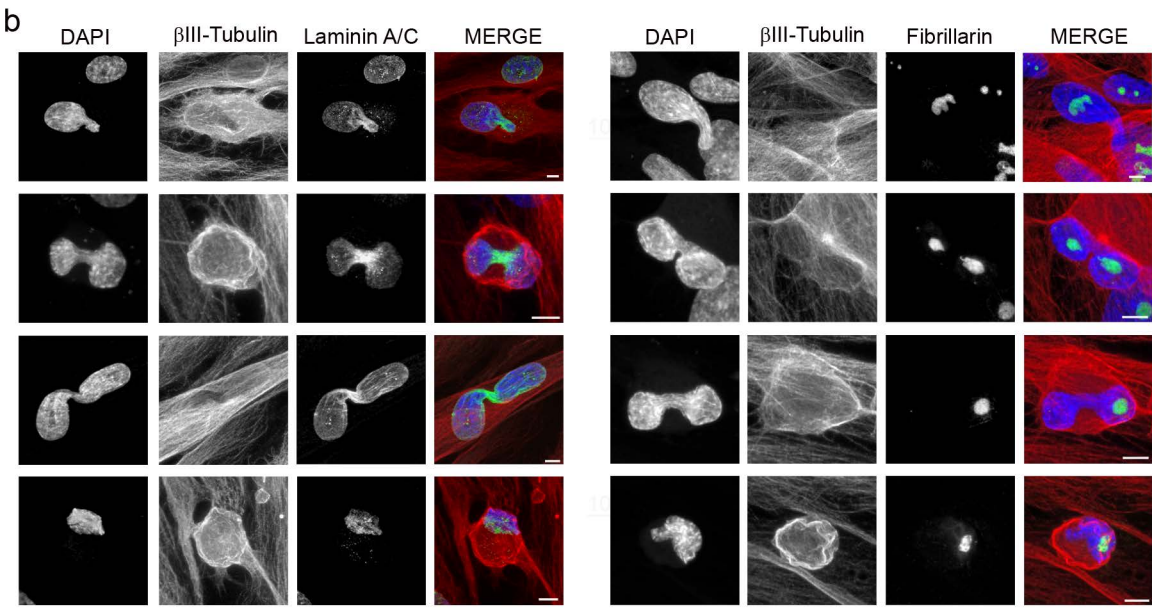
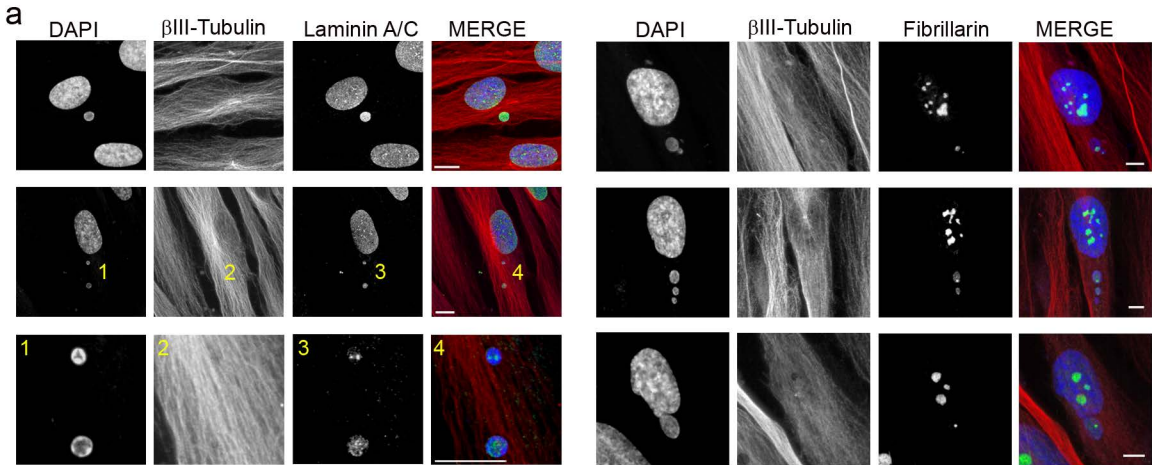


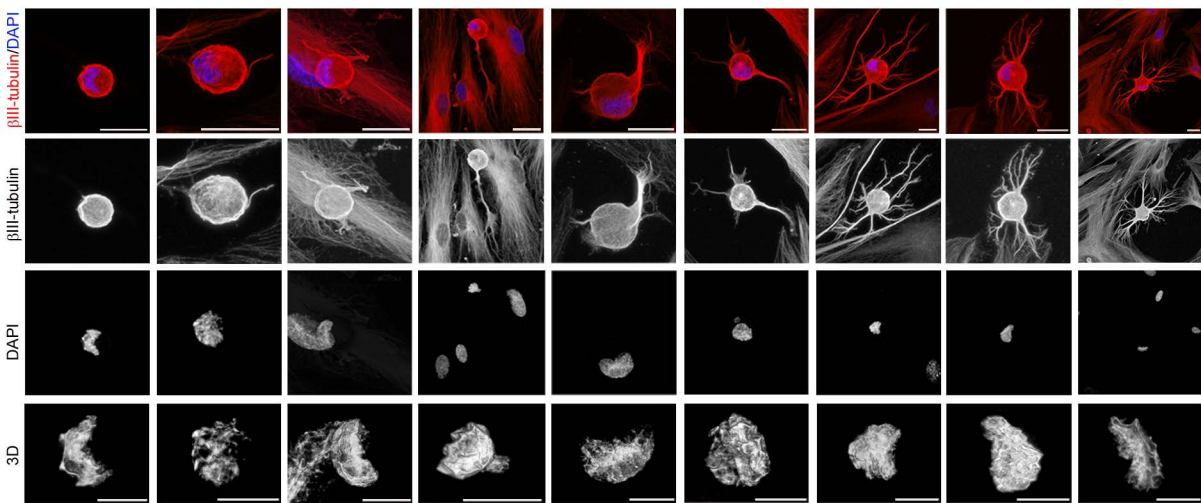
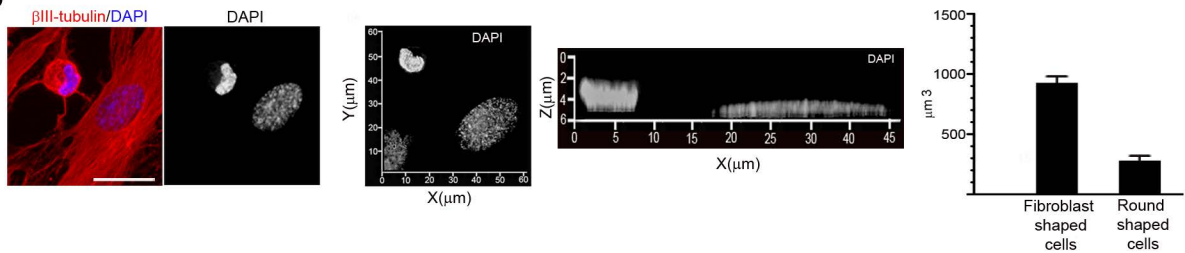
a**b**



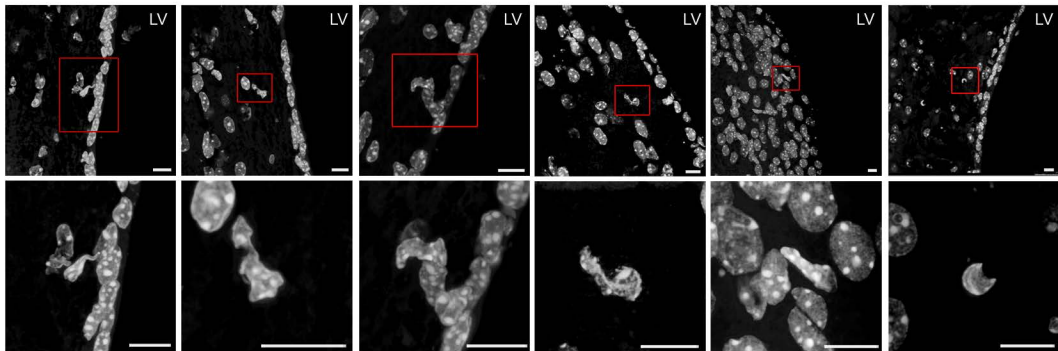


a β III-tubulin/DAPI β III-tubulin β III-tubulin/DAPI β III-tubulin β III-tubulin/DAPI β III-tubulin β III-tubulin/DAPI β III-tubulin**b** β III-tubulin/DAPI β III-tubulin β III-tubulin/DAPI β III-tubulin β III-tubulin/DAPI β III-tubulin β III-tubulin/DAPI β III-tubulin



a**b**

a



b

